Attachment 6

Vermont Yankee Nuclear Power Station

Proposed Technical Specification Change No. 263 – Supplement No. 26

Extended Power Uprate

Steam Dryer Analyses and Monitoring

GE-NE-0000-0038-0936-NP Vermont Yankee Nuclear Power Station Modified Steam Dryer Stress Analysis

Non-Proprietary Version

Total number of pages in Attachment 6 (excluding this cover sheet) is 54.

GE-NE-0000-0038-0936-NP
Class I
DRF Section 0000-0038-0936
March 2005

Non-proprietary Version

Entergy Nuclear Operations Incorporated

Vermont Yankee Nuclear Power Station Modified Steam Dryer Stress Analysis

Principal Contributors:

H. S. Mehta
I. Shekhtman

Principal Verifier:

H.L. Hwang

Manager:

Mike Schrag

NON PROPRIETARY NOTICE

IMPORTANT NOTICE

This is a non-proprietary version of the document GE-NE-0000-0038-0936P, which has the proprietary information removed. Portions of the document that have been removed are indicated by an open and closed bracket as shown here [[ ]].

IMPORTANT NOTICE REGARDING THE CONTENTS OF THIS REPORT

Please Read Carefully

The only undertakings of the General Electric Company (GE) respecting information in this document are contained in the contract between Entergy Nuclear Operations Incorporated and GE, Order 4500528282, Schedule A-2, as amended to the date of transmittal of this document, and nothing contained in this document shall be construed as changing the contract. The use of this information by anyone other than Entergy Nuclear Operations Incorporated, for any purpose other than that for which it is furnished by GE, is not authorized; and with respect to any unauthorized use, GE makes no representation or warranty, express or implied, and assumes no liability as to the completeness, accuracy, or usefulness of the information contained in this document, or that its use may not infringe upon privately owned rights.

Table of Contents

List of Figures

List of Tables

1.0 Executive Summary

As a result of BWR/3 steam dryer failures in the industry, Entergy has performed a comprehensive structural evaluation to demonstrate the adequacy of the Vermont Yankee (VYNPS) dryer integrity for extended power uprate (EPU) steam flow changes. The key issue has been the modeling of the flow-induced vibration (FIV) loading during normal operation.

The purpose of the analysis reported here is to update the FIV stresses using pressure fluctuating loads generated with the combination of an acoustic circuit model and a computational fluid dynamics (CFD) large eddy simulation (LES) model for vortex shedding. The acoustic circuit model, LES model and resulting alternating stresses will provide Entergy with a more realistic load definition and a basis to systematically monitor changes to predicted dryer stresses during power ascension to EPU conditions.

The VYNPS acoustic circuit model was developed based on plant design/operation configuration and used VY-specific measured pressure fluctuation data as input. The acoustic circuit methodology was benchmarked with scale model test results developed by GE for Entergy. The LES model characterizes the nature and magnitude of unsteady flow effects across the face of the dryer at the entrance to the main steam line nozzles. Each model generated time history pressure profiles that were input to the ANSYS finite element program to determine associated FIV stresses.

Maximum acoustic pressure stresses and vortex shedding stresses were extracted from separate finite element analyses. The stresses were conservatively combined and, where appropriate, multiplied by stress concentration factors that account for weld shape and size. The time history analysis was done with a +/-10% time step change to conservatively account for uncertainty in the frequency content of the FIV loads.

The resulting maximum FIV stresses calculated for current power were about 25% of the 13,600 psi ASME endurance limit. In addition, normal, upset and faulted stresses were calculated and compared to ASME Code allowable, with all conditions showing acceptable stresses.

2.0 Background and Introduction

As a result of significant steam dryer cover plate fatigue cracking at Quad Cities Unit 2, GE issued SIL 644 in August of 2002 to provide information to all BWR utilities on cover plate related failures. In September of 2003, GE added Supplement 1 to SIL No. 644 in order to describe additional steam dryer fatigue cracking at Quad Cities 2, and to explain that the root cause of the second event was different than the first. SIL 644 applied to BWR/3-style steam dryer design plants. Supplement 1 to SIL No. 644 provided recommendations applicable to plants with BWR/4 and later design steam dryers. The objective of this report is to detail the latest analyses of the Vermont Yankee Nuclear Power Station (VYNPS) steam dryer that were performed for the modified dryer configuration. The purpose of these analyses is to confirm that the modified dryer meets ASME criteria for fatigue initiation and other ASME-based design criteria.

The VYNPS steam dryer modifications included replacing the ½ inch outer vertical plates and portions of the top hood plates with 1-inch plates, removing internal brackets that attached the internal braces to the outer hood plates, replacing the ¼ inch thick cover plate with 5/8 inch thick material, and adding three long gussets at the outer vertical hood plate and cover plate junction. Each gusset is triangular in shape, 53 inches high, with no more than 1.0-inch width at the top. The top of each gusset is welded around and has a smooth transition to the modified front hood. Each gusset extends to within 5.5 inches of the top of the modified front hood. Transition between each gusset and the modified lower cover plate is accomplished via the use of a U-shaped "gusset extension" that is welded to both the lower cover plate and to each gusset. The replacement lower cover plate is attached with 1/2-inch welds all around except for the corner intersection with the dryer support ring where 5/8-inch welds are used for a distance of four inches. The existing tie-bars are replaced with a modified tie bar design. Figures 2-1 and 2-2 show the modified dryer configuration.

A brief summary of the previous analyses done is provided as background for the analysis results documented in this report. Reference [1] documents a stress analysis of the modified dryer based on equivalent static load methodology. The equivalent static pressure was based on the estimated pressure fluctuations on the dryer faces and an estimated dynamic amplification factor. In order to address the dynamic amplifications explicitly and to account for the sensitivity in modal frequency variations, a response spectrum approach based analysis was documented in [2]. However, the enveloping load definition used in this approach led to very high fatigue stresses such that fatigue failures were predicted at locations where the field history had shown no such failures. Therefore, a scale factor developed consistent with known field failures had to be used to calculate realistic values of fatigue stresses. A review by the NRC [3] found this technical approach to be inadequate in that the scaling factor may not be the same at

various locations in the dryer. Several other deficiencies in that analysis were also identified in [3] (e.g., need for adding FIV primary stress in the ASME load combinations and consideration of loads due to a postulated break in the steam line outside the containment). The NRC review also identified the need for a plant specific identification of acoustic and other fluctuating pressure loading sources.

The analysis presented in this report addresses the deficiencies identified by the NRC audit. Specifically, an acoustic circuit model was used with VY-specific plant signals to develop acoustic loading on the dryer. This analysis and the ENVY steam dryer ascension test monitoring accounts for acoustic sources that may impact the dryer. Additionally, vortex-induced loading on the front face of the dryer was also estimated through a transient CFD analysis. The stresses from the two sources were then combined to obtain total FIV fatigue stresses.

The acoustic model includes the affect of unsteady flow forces that originate at the exit to the vessel and the CFD model includes compressible flow and therefore accounts for vortex pressure forces. The addition of both sets of loads is conservative. The advantage of using both sets of loads is that the CFD model provides a more detailed assessment of unsteady dryer loads along the face of the dryer. Therefore lateral loads on the gussets and local vortex pressure gradients are considered. The acoustic model accounts for external piping acoustic pressures from plant data. The CFD model provides more conservative low frequency loads and the acoustic model provides more conservative high frequency loads. Therefore the addition of these load cases applies conservatism in both magnitude and frequency content for the FIV load.

The purpose of the analysis reported here is to update the current licensed thermal power (CLTP) analysis using pressure fluctuating loads generated with the combination of an acoustic circuit model for acoustic pressures and a large eddy simulation (LES) model for vortex shedding pressures. The acoustic circuit model, LES model and resulting alternating stresses will provide Entergy a basis to systematically monitor changes to dryer stresses while they increase power to extended power uprate (EPU) conditions.

[[

]]

Figure 2-1 Modified Dryer

[[

]]

Figure 2-2 Modification Details

3.0 Dryer Analysis Approach

The analysis presented follows the same approach as described previously for the modified dryer, except in the area of fatigue stresses, where the loads and the method of applying those loads to the finite element analysis (FEA) model have been updated.

3.1 Operational Pressure Loading

The flow-induced vibration (FIV) loading as a result of the passage of steam through the steam dryer vane banks is a significant cyclic loading that has the potential to initiate and grow fatigue cracking. This FIV loading in the form of distributed fluctuating pressures is highly complex in that it varies as a function of the location and phasing, and has complex frequency content. The first analyses of the modified dryer [1] used an equivalent static pressure approach to represent the FIV loading. The second analysis [2] used a response spectrum based on four instrumented dryer plants' measured pressure time histories, applied to VYNPS with a scaling factor based on steam line velocity differences. However, both technical approaches were judged inadequate from the point of view of actual plant loadings.

In the updated analysis, the FIV pressure loading was calculated from two sources: (1) Acoustic Circuit Modeling, and (2) Large Eddy Simulation (LES). The total FIV pressure loading is represented by a combination of acoustic pressures and vortex shedding pressures. These pressure loads were provided by Entergy. Brief overview descriptions of the acoustic circuit model and the LES model are provided herein. The methods used to apply the pressures to the ANSYS FEA model are described as well.

3.1.1 Acoustic Pressures

The acoustic circuit based pressure fluctuations were developed by Continuum Dynamics Inc. (CDI) [4] and supplied by Entergy as input to GE. The acoustic circuit model for the VYNPS steam path (i.e., steam dome, dryer and the steam lines) was developed by CDI and used VY-specific measured pressure fluctuation data as input. The ability of the acoustic circuit model to predict dryer pressure loads from main steam system fluctuating pressure measurements was benchmarked with scale model test results by Entergy [5]. The acoustic circuit model loads were applied to the GE finite element model of the dryer as time varying pressure vectors.

The CDI acoustic model solved for pressures in the RPV dome with a 3"x3" detailed grid. Differential pressures on components in the area of the dryer front face were then calculated at a 3x3 inch mesh. Based on discussion with GE, CDI provided coarser 6"x6" and 12"x12" summaries in areas away from the face where fluctuating loads were much lower and the pressure gradients permitted less refined grid information. This variable load grid help optimize the data processing efficiency of ANSYS load vectors.

Based on the CDI model and Grid information GE then developed an ANSYS Macro to translate the CDI supplied pressures into input pressures for the GE ANSYS finite element model. This macro was checked by comparing the resulting ANSYS load vectors at 28 key locations in the dryer against the CDI loads. The comparisons showed that the ANSYS load vectors and CDI pressure fluctuations matched, or that the ANSYS values were conservative.

3.1.2 Vortex Shedding Pressures

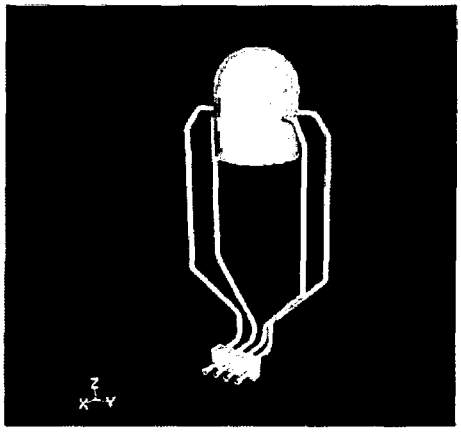

Entergy has performed a CFD LES compressible flow simulation of the VY dryer. The purpose of this model is to assess vortex shedding and other unsteady flow effects along one face of the dryer and into the main steam nozzles. The CFD model was developed by Fluent and includes the dryer RPV dome and main steam piping to the steam equalizer approximating the total pressure loss in the system. This model includes a detailed refined mesh along one side of the dryer. This is depicted as the foreground in the pressure contour plots shown below. The balance of the model includes sufficient detail to simulate flow throughout the vessel dome and piping. This lower resolution portion of the model was required to assure flow in and out of the front face region was depicted accurately.

The purpose of this model is to characterize the nature and magnitude of unsteady flow effects across one face of the dryer at 100% CLTP conditions. This CFD model is very large. It has nearly 4.5 million cells and on a system with up to 12 parallel processors requires a full day to produce about 0.7 second of simulation.

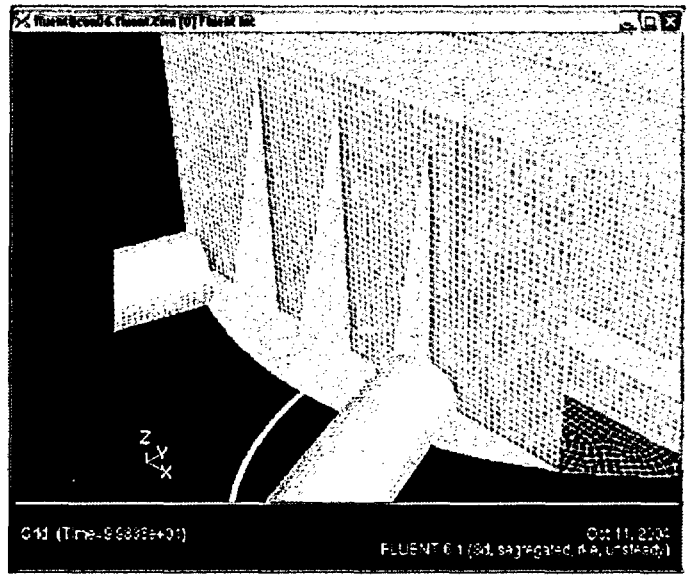

Included in Figure 3.1-1 is an example of figures that depict differential pressure across major plate components of the VY dryer at 17 time points (at roughly 0.25 second intervals). These contour plots provide a good sense of how the predicted differential pressure variation changes with time. In general it can be noted the more severe pressure gradients are adjacent to the steam nozzles. These are caused by a vortex as the steam exits the vessel. This vortex forms then disappears then reappears less pronounced at the adjacent nozzle. In earlier CFD analysis performed with a clipped domain incompressible LES solution it was noted that after 8 seconds the vortex pressure oscillations subsided. It is likely that with more time, some of the oscillations currently observed with this much larger model may also subside.

In general the other contours away from the nozzle do not undergo significant change. The dryer face is subject to a ~0.8 psi pressure differential as the higher pressure, slower moving steam within the dryer comes over the top and accelerates into the steam nozzles. The 17 snapshots of data presented here are just a data sample and not continuous record. After eight months of model development and months of computer time, this CFD results permit quantification of the impact of CFD loads variations on dryer fatigue.

In the fatigue assessment for CFD loads, the alternating stress caused by the unsteady CFD differential pressures was evaluated. The CFD model provides ~18,000 pressure values across the vertical plate and ~2500 element areas of the two outer gussets. Therefore to help interpret the delta-P data we have provided three graphs, Figures 3.1-2 through 3.1-4. These graphs depict both the average pressure and maximum pressure differential across the vertical plate, the left gusset, and right gusset. These are the components most affected by the CFD forces. The coming and going of the vortex

directly impacts the maximum pressure differential across each component. The change in average pressure impacts the ballooning of the vertical face and gussets.

The large changes in the vortex movement occur very slowly. The low pressure regions and high differential pressures take over a second to change. In addition to the very slow vortex changes, there are much lower magnitude, higher frequency changes occurring also. Entergy has generated detailed pressure data on the dryer face at a 0.0005 sec interval (2000 Hz). The power spectral density (PSD) plots, for this data are included in Figure 3.1-5.

Point 6 represents frequency content close to the vortex. The vortex forces have negligible impact to the 1" dryer face and 5/8" cover plate. The vortex pressures do have a localized effect resulting in lateral bending loads on the gussets. This would impact the 2nd mode natural frequency of 99 Hz of the gussets[1]. The majority of the Point 6 energy is below 45 Hz.

3.2 Time History Analysis with Modal Superposition

The dynamic structural response of the dryer to the applied pressure fluctuations from acoustic loading was calculated using a time history method with modal superposition. Normal modes up to 200 Hz were included in calculating the response. Entergy has collected transient data during multiple full power operation periods. CDI used a representative 16 second set of data and performed a coarse transient solution. GE requested that Entergy provide approximately 2 seconds of transient fine mesh data for their analysis. Therefore CDI provided a 2.4 second subset of fine mesh data that contained the highest Prms and peak data of their 16-second analysis. The plant data acquisition for the strain gages and pressure transmitters was at 1024 Hz and 2000 Hz respectively. From this data, CDI developed the dryer transient data at 1024 Hz time rate. The selection of modes up to 200 Hz in the modal superposition analysis is consistent with the preceding time interval between the acoustic pressure values and captures the important mode shapes that contribute to fatigue stress in the model.

3.2.1 Time Step Selection and Sensitivity

The time step value used in the time history analysis was 0.000977 second. It is an accepted engineering practice to assess the sensitivity of the calculated stresses to such factors as differences in modal frequency due to geometric and material variations,

[1] GE-NE 000-0026-7944-1 pgs 44, Vermont Yankee Nuclear Power Station Steam Dryer Modification, Revision 1, March 2004.

random variations in pressure time history, etc. A sensitivity assessment was conducted by varying the time interval between the pressure time steps by [[ ]]. This is equivalent to peak broadening in the response spectrum analysis method. The [[ ]] variation was judged to be a reasonable value to capture instances where a structural mode that contributes significant response may have its frequency very close to any one of the frequencies present in the fluctuating pressure time history. The ENVY Acoustic Model Benchmark Report [5] demonstrates that the [[ ]] variation provides a conservative envelope of transient data. For dryer components with the higher FIV stresses and positive changes in stress intensity with time step change, the FIV stress increase was assessed relative to the endurance limit.

3.2.2 Damping

A conservative damping value of [[ ]] of the critical damping was used in the modal superposition analysis. Technical justification for the selection of this value is provided in [6]. This value was applied uniformly for all the modes.

3.3 Model Material Properties

The original VYNPS dryer assembly was manufactured from solution heat-treated SS304 conforming to applicable ASTM standards at the time of manufacture. The modification plate is made from SS316L. Minimum of SS304L and 316L properties from [7] were used to conservatively envelop the properties of the unmodified components and the modification plate. In actuality the stress intensity limit, S_m, of SS304 is slightly greater than SS304L[2]. Therefore the use of SS304L material properties for unmodified dryer components is conservative. The applicable properties are shown in Table 3.3-1.

[2] The ASME code 1971 and 1989 editions have the following material properties for SS304:
ASME 1971 – S_m = 17.4 ksi at 500°F, S_m = 16.4 ksi at 600°F
ASME 1989 – S_m = 17.5 ksi at 500°F, S_m = 16.4 ksi at 600°F

Table 3.3-1 Properties of SS304L and SS316L

Material / Property	Room temperature 70°F	Design temperature 575°F
SS304L		
S_m, Stress intensity limit, psi	16700	14,200
S_y, Yield strength, psi	25000	15,700
S_u, Ultimate strength, psi	70000	57,200
S_{alt}, Endurance limit, psi		13,600
E, Elastic modulus, psi	28300000	25575000
SS316L		
S_m, Stress intensity limit, psi	16700	13,725
S_y, Yield strength, psi	25000	15,225
S_u, Ultimate strength, psi	70000	61600
S_{alt}, Endurance limit, psi		13,600
E, Elastic modulus, psi	28300000	25575000

3.4 Design Criteria

The analysis uses the ASME Code [8] as a design guide although the dryer is not an ASME Code component. Specifically, structural adequacy for Service Level A and B loads was investigated using the corresponding stress limits of [8] with the exception of application of the weld quality factors. Weld quality factors are described in the ASME code Table NG-3352-1 for safety components, such as the reactor pressure vessel, that contain radioactive fluid. Because the steam dryer is not a safety-related pressure retaining component [[

]] The requirement of 'no loose parts' during Service Level D events was investigated using stress limits of Subsection NG and Appendix F of the ASME Code [9]. The stress limits are summarized in Table 3.4-1. (Note that for completeness, application of the seismic loading in the [[ ]] direction was considered).

Table 3.4-1 Primary Stress Limits

Service level	Stress category	Stress limit
Service levels A & B	P_m	S_m
	$P_m + P_b$	$1.5\ S_m$
	Shear stress	$0.6\ S_m$
	Bearing stress	$1.5\ S_y$
	Σ fatigue damage	1.0
Service level D	P_m	min ($2.4S_m$, $0.7S_u$)
	$P_m + P_b$	min ($3.6S_m$, $1.05S_u$)
	Shear stress	$1.2\ S_m$
	Bearing stress	$3.0\ S_y$

P_m: Primary membrane stress intensity
P_b: Primary bending stress intensity
S_m: Stress intensity limit
S_y: Yield strength
S_u: Ultimate strength

3.5 Dryer Loads

3.5.1 Transient Pressure Loads

The FIV pressure loading on the dryer components is described in Section 3.1. The other normal operating and transient pressure loadings on the dryer components for other service conditions are described for EPU conditions in Appendix A. They are used here as conservative CLTP loads.

3.5.2 Seismic Loads

The seismic loads on the VYNPS dryer are documented in [10]. These seismic loads are unchanged with EPU, were used in the [1] and [2] evaluations and are used here. The accelerations are listed below.

[[

]]

Because the modified dryer first mode frequency is in the ZPA (Zero Period Acceleration) range of the seismic load ([[ ]]), the time history maximum acceleration (g) load is the dryer acceleration (g) load considered in a static analysis.

3.6 Load Combinations

The VYNPS steam dryer was originally procured and supplied as a non-safety related, non-seismic category I, non-ASME component. There was no design specification for the dryer and, as such, the service conditions for the steam dryer were not specifically defined. However, as late as 1969, an internal GE design report, 257HA760, was prepared for BWR-3 style steam dryers. In the 257HA760 report the following service condition and acceptance criterion were stated:

- The principal design loads considered in the analysis of the steam dryer assembly are the weight loads and the pressure loads, which are present during accident conditions.
- In the event of a guillotine steam line break outside the drywell, dryer design must preclude the possibility of dryer debris entering the steam line and interfering with isolation valve closure.
- The structural elements, which hold the dryer in place, are designed to accommodate the pressure loading due to a break outside the isolation valves within the ASME Code, Section III stress criteria. The flat panels, which form partitions in the dryer,

are designed so that the elastic collapse loading on these panels is not exceeded under these same pressure loadings.

The above criteria continue as design bases for the modified VYNPS steam dryer, both at CLTP and EPU conditions. The VYNPS steam dryer design basis continues to be structural integrity after a steam line break outside of containment. However, due to the operating experience related to steam dryer structural integrity associated with normal operation, this analysis includes Normal and Upset case loading combinations. Analysis of Normal and Upset cases addresses the concern that frequent and moderately frequent events which do not require an immediate inspection of the dryer should not degrade the dryer condition to the point that it might not meet its Level D design criteria.

Table 3.6-1 provides the load combinations and load cases used in the VYNPS dryer analysis.

Table 3.6-1 ASME Code Section III Load Combinations

Case	Service Level	Load Combination
[[		

]]

3.7 FEA Analysis Model

Transient and static stress analyses were performed using the ANSYS finite element code (Versions 6 and 8) running under Windows 2000 Operating System [11]. The model is a full dryer model, as shown in Figure 3.7-1, which incorporates the modifications made to the VYNPS dryer in 2004. To allow more efficient time history execution, the model in [12] was simplified by effectively removing the detailed tie bar and steam dam repair modeling on the top hood. The half of the model without these details was replicated by symmetry to replace the half with the details.

In final verification of the model and completed analysis cases, one node was found in the modified hood that was inappropriately constrained by the beam below. The node was corrected and a static case run to assess the stiffness changes. The modified hood stress decreased as a result and the attached end plate stress increased. FIV stresses were scaled accordingly in these two components.

3.8 FIV Stress Determination

The FIV stresses are taken as a combination of the acoustic and vortex shedding contributions. The acoustic pressure FEA results for each dryer component of interest are screened for the maximum stress intensity throughout the ~2500 time steps. The stress intensity is conservatively used as the acoustic contribution to the FIV stress amplitude.

Because the majority of the vortex shedding load energy is well below the natural frequency of the affected components, static analysis alone provides a reasonable assessment of alternating stress and fatigue impact under the changing pressure loads described in Section 3.1.2. Therefore, the ANSYS FE model of the dryer was first used to statically assess the pressure cases to determine the magnitude of the CFD load related alternating stresses. Based on review of the pressure contours and preliminary static stress analyses, Entergy selected 7 of the 17 cases, which represent the key load conditions for the determination of representative alternating stress ranges. The conditions selected for ANSYS analysis included 100% CLTP time steps at 2.20sec, 3.20 sec, 4.45 sec, 4.70 sec, 4.95 sec, 5.20 sec, and 5.23 sec.

Based on the ANSYS results the following 10 load case combinations for the alternating stress calculation were selected:

1. 2.20 sec to 3.20 sec
2. 2.20 sec to 5.23 sec
3. 3.20 sec to 5.20 sec
4. 3.20 sec to 5.23 sec
5. 4.45 sec to 4.70 sec
6. 4.45 sec to 5.20 sec
7. 4.70 sec to 4.95 sec
8. 4.70 sec to 5.20 sec
9. 4.95 sec to 5.20 sec
10. 4.95 sec to 5.23 sec

These cases are selected to maximize alternating stress but also biased to later time points under the assumptions that as time progressed the CFD model would be converging on a steady state solution.

The stress intensity from the acoustic pressure analysis is added by absolute sum to the maximum stress range from the vortex shedding pressure analysis. This is conservative because the acoustic stress intensity is larger than the maximum acoustic FIV stress of interest and because the acoustic and vortex shedding maximum stresses likely do not occur at the same location in the component.

3.9 Weld Stress Concentration Factors

The following stress concentration factors (SCFs) were used in this evaluation: [[ ]] These SCFs were applied to the calculated peak stresses from the finite element analyses. The use of peak stress to multiply with SCFs provides alternating stresses at welds consistent with recommended SCFs in the ASME Code. The technical basis for these values is provided in [13]. These values are also consistent with those used in the previous stress analyses for VY dryer (e.g., [1]).

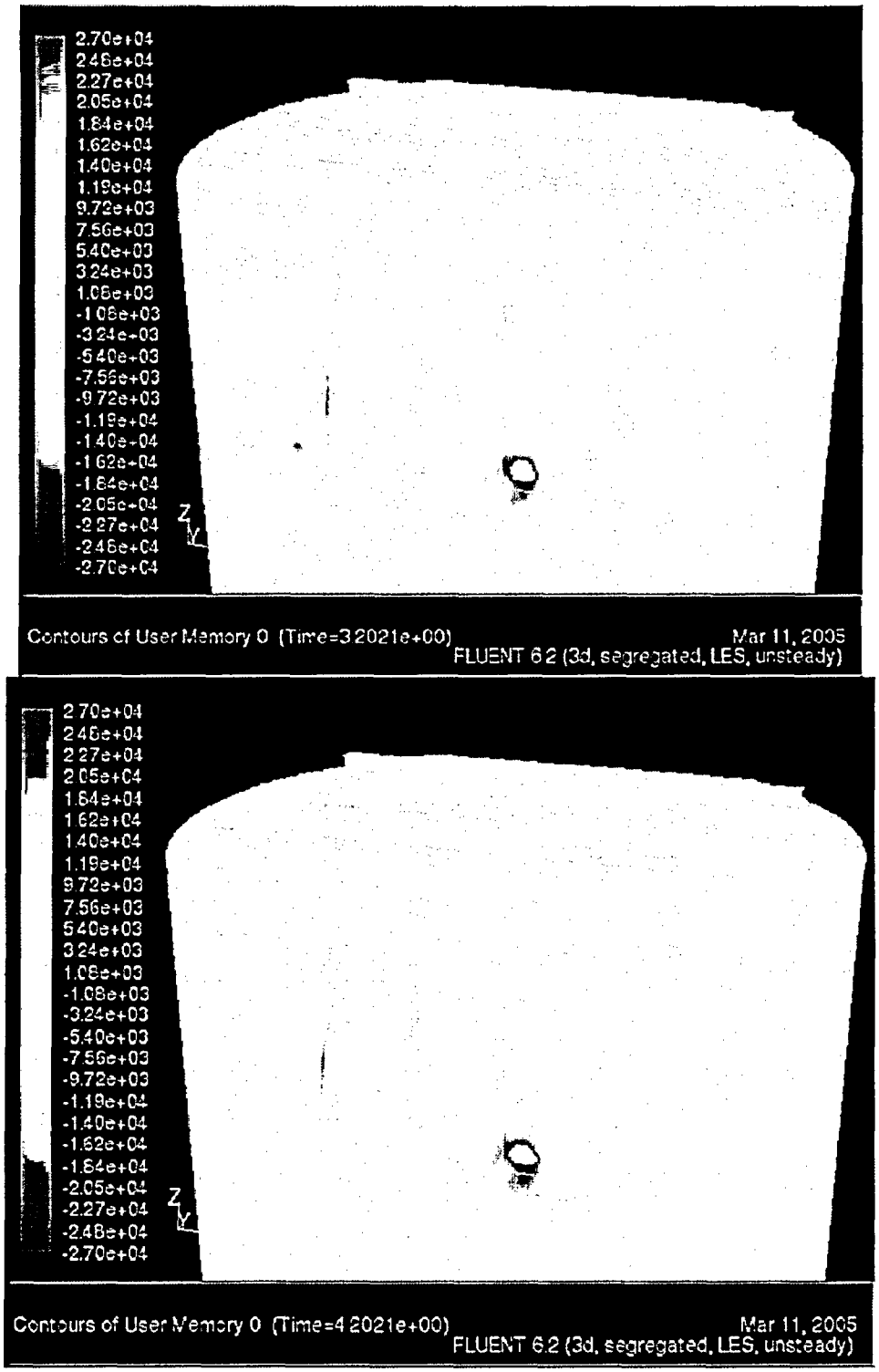

Figure 3.1-1 Examples of Pressure Contour Plots

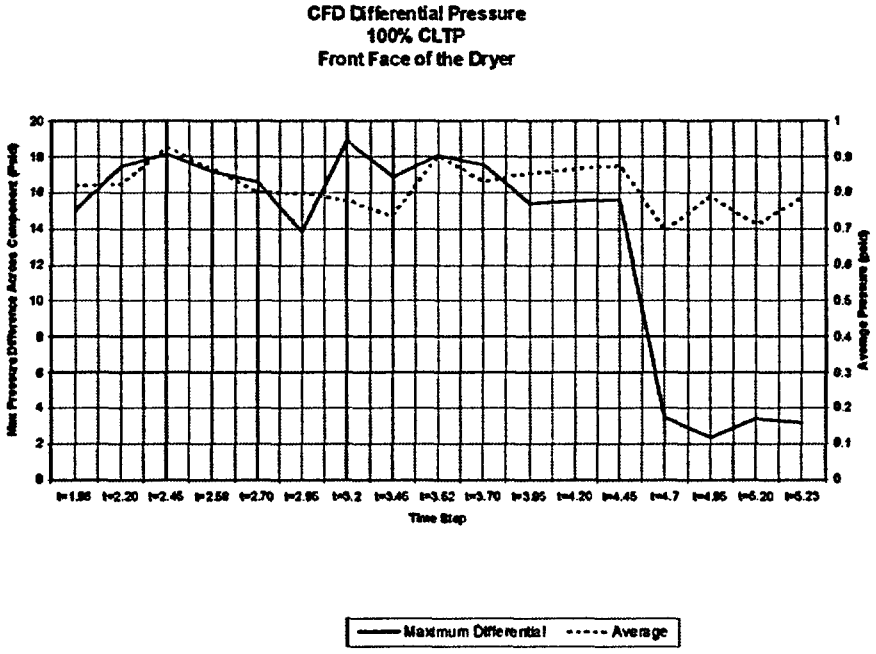

Figure 3.1-2 Pressure Differential Across Vertical Plate

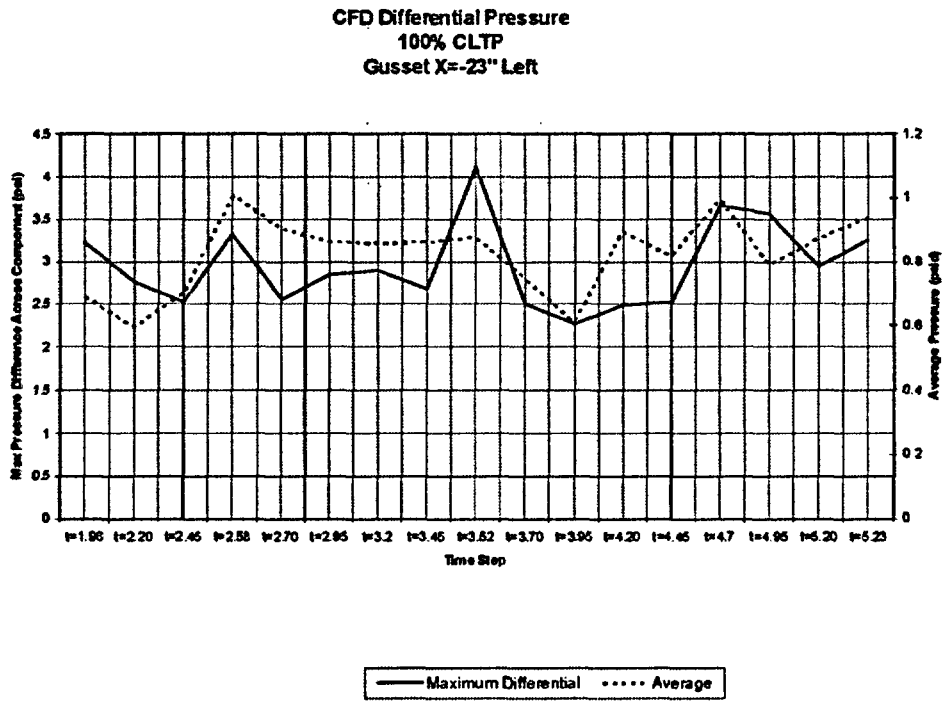

Figure 3.1-3 Pressure Differential Across Left Gusset

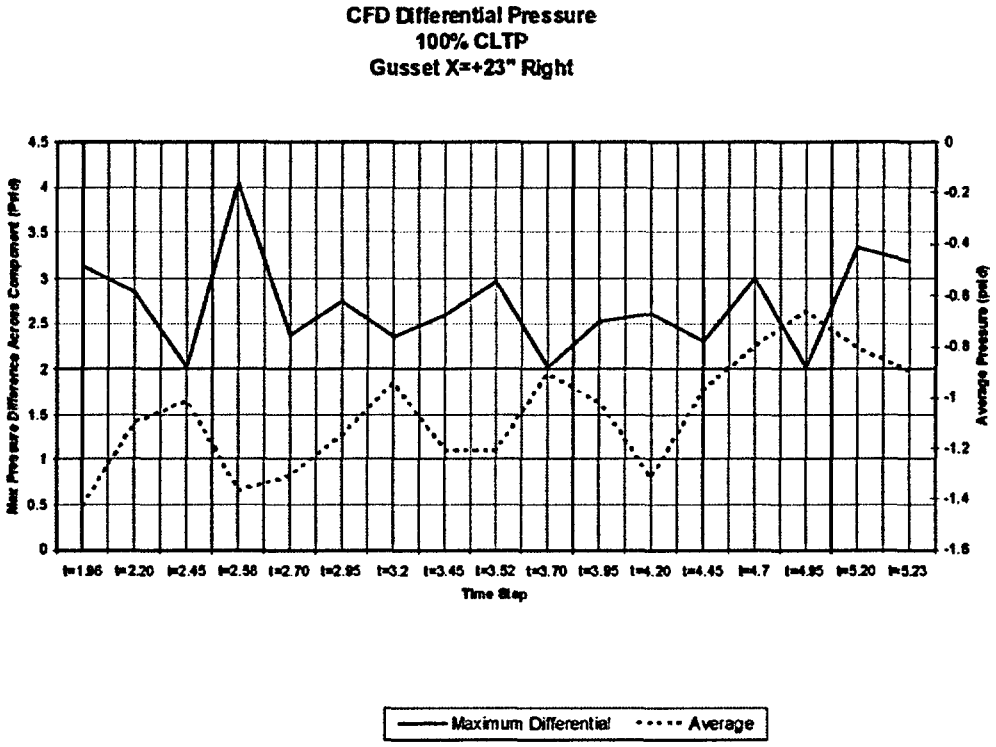

Figure 3.1-4 Pressure Differential Across Right Gusset

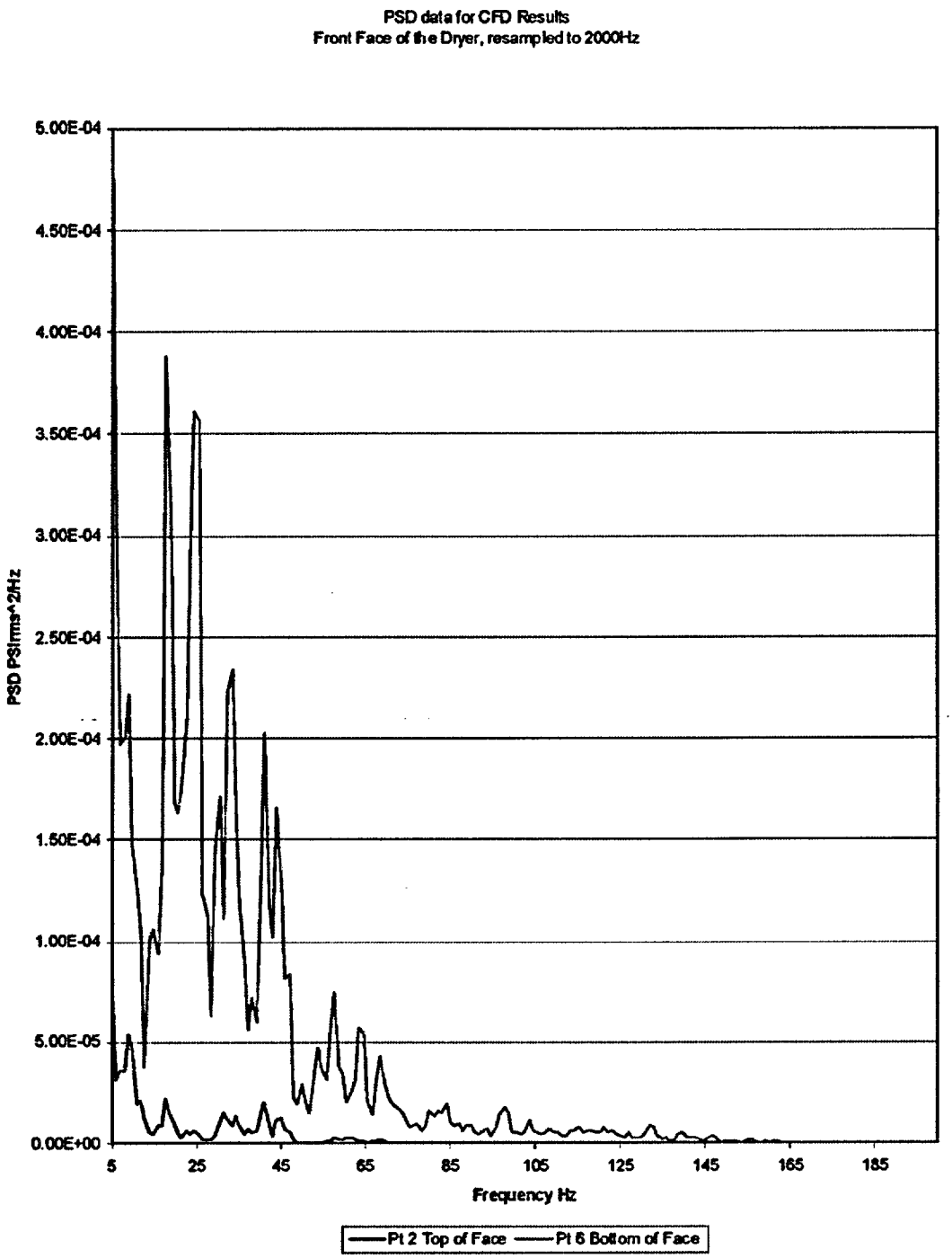

Figure 3.1-5 PSD for Point 6 of LES Model

[[

]]

Figure 3.7-1 Modified Full Dryer Analysis Model

4.0 Modified Dryer Analysis Results

4.1 Acoustic Pressure Stresses

The ANSYS model produces stress intensities from the acoustic pressure zero-to-peak amplitudes. Stress intensity contour plots for each component are included in Appendix B. The maximum stress intensity for each component was extracted from the analysis for use in Table 4.4-1. The applicable primary stresses from the extractions were used as part of the primary stress evaluation for the components shown in Section 4.3.

4.2.1 Sensitivity Results

Table 4.2-1 shows the relative change in maximum stress intensity for the acoustic pressure stresses as a result of the [[ ]] time step changes. In a couple of instances, the stresses increased in the [[ ]] time step case. The potential impact to FIV results for these increases is discussed in Section 4.4.

4.2 Vortex Shedding Stresses

The 10 load case combinations described in Section 3.8 were screened for the maximum surface stress range for each component. Then from the 10 maximum results, the largest was selected to combine, as an amplitude, with the acoustic stress intensity value in Table 4.4-1. The vortex shedding maximum stress may not occur at the same location as the acoustic pressure maximum stress, so this is an additional conservatism in the FIV stresses.

4.3 Evaluation of Primary Stresses under ASME Code Section III Loads

Each of the load combination tabulated in Table 3.6-1 has been analyzed for the modified dryer in [1]. With the exception of the FIV stresses, the other stresses are calculated for EPU conditions, which is conservative across the board for CLTP evaluation. In the ASME Code Section III load analysis, the dynamic loads, such as OBE, SSE and TSV loads should be combined by square root of the sum of the square (SRSS). This analysis combined the dynamic loads by algebraic sum. Because the OBE and SSE have been input in both the positive and negative directions and both results are compared with the allowable limits, the results are equivalent to absolute sum results. Therefore, the load combinations are conservative. The TSV pressure impulse load has been multiplied by a dynamic load factor of 1.5 in the input for ANSYS analyses.

Tables 4.3-1 through 4.3-7 tabulate the stresses for each weld with the undersize weld factor included. The maximum stress ratio is 0.76, at the gusset, due to the Service Level B-3 load combination. There is more than 20% margin for any ASME Level A or Level B load combination.

4.4 Evaluation of FIV Stresses vs. Endurance Limit

Table 4.4-1 shows the CLTP acoustic and vortex shedding maximum stress amplitudes for each key dryer component. These stresses are conservatively combined by absolute sum and the sum is multiplied by the weld undersize factor and the weld stress concentration factor to determine the FIV stress on each component. The maximum value for CLTP conditions is well below the endurance limit.

If the stress increases to acoustic stress of the increased time step are factored into the FIV stresses, the results are the values in Table 4.4-2.

The FEA for FIV stresses is a linear analysis, so the Entergy approach of monitoring main steam system fluctuating pressure measurements during power ascension to EPU conditions, in accordance with the VYNPS Steam Dryer Power Ascension Test Plan (SDPATP) is appropriate using these results. If predicted dryer FIV pressures approach the endurance limit, FEA can be employed to determine FIV stresses.

Table 4.2-1 Time Step Sensitivity Results

[[

]]

Table 4.3-1 Modified Dryer Stresses at the Outer Cover Plate

[[

]]

Table 4.3-2 Modified Dryer Stress at the Original Front Hood Both Side Strips

[[

]]

Table 4.3-3 Modified Dryer Stress at the 1.0 Inch Front Hood Lower Weld

[[

]]

Table 4.3-4 Modified Dryer Stress at the Unmodified Top hood

[[

]]

Table 4.3-5 Modified Dryer Stress at the 1" Thick Top hood

[[

]]

Table 4.3-6 Modified Dryer Stress at the Long Gussets

[[

]]

Table 4.3-7 Modified Dryer Stress at the Vertical Side Hood

[[

]]

Table 4.4-1 FIV Stress Summary, Nominal for CLTP

[[

]]

Table 4.4-2 FIV Stress Summary, +10% Time Step

[[

]]

5.0 Conclusion

5.1 Fatigue Alternating Stresses

The FIV alternating stresses shown in Table 5.1-1 are well below the endurance limit. Similarly, the FIV alternating stresses for a [[ ]] time step in Table 5.1-2 are below the endurance limit of 13,600 psi.

Table 5.1-1 FIV Stresses for Key Dryer Components

Item	Current FIV Results (psi)	Endurance Limit (psi)
Front Vertical Hood Bottom Weld	2,222	13,600
Front Hood Gusset Weld	3,238	13,600
Front Vertical Hood Top Weld	2,417	13,600

Table 5.1-2 FIV Stresses ([[ ]] Time Step) for Key Dryer Components

Item	Current FIV Results (psi)	Endurance Limit (psi)
Front Vertical Hood Bottom Weld	2,810	13,600
Front Hood Gusset Weld	3,535	13,600
Modified Hood Top Hood	2,900	13,600

5.2 ASME Primary Stresses Evaluation

The modified dryer meets the ASME Code Section III, Service Level A, B, C and D, primary stress criteria for all the load combinations tabulated in Table 3.6-1 using conservative methods of analysis.

6.0 References

[1] GE-NE 0000-0024-7944-1, Vermont Yankee Nuclear Power Station Steam Dryer Modification, Revision 1, March 2004.

[2] GE-NE 0000-0024-7944-3, Vermont Yankee Nuclear Power Station Steam Dryer Dynamic Response Spectrum Analysis, Revision 0, June 2004.

[3] Docket No. 50-271, Technical Audit of Vermont Yankee Steam Dryer Analysis in Support of Extended Power Uprate Request, USNCR, August 24-26, 2004.

[4] C.D.I. Technical Memorandum No. 05-06, Analysis of Steam Dryer Differential Pressure Loads at Vermont Yankee, Revision 0

[5] Entergy Engineering Report No. VY-RPT-05-00006 Rev 0, Acoustic Model Benchmark, Dryer Acoustic Load Methodology, 3-29-2005

[6] Wu, Richard, Damping Value for Steam Dryer Dynamic Analysis, GE eDRF 0000-0034-1855, November 2004.

[7] American Society of Mechanical Engineers (ASME) Boiler and Pressure Vessel Code, Section III, Appendix I, 1989 Edition with no Addenda.

[8] American Society of Mechanical Engineers (ASME) Boiler and Pressure Vessel Code, Section III, Subsection NG, 1989 Edition with no Addenda.

[9] American Society of Mechanical Engineers (ASME) Boiler and Pressure Vessel Code, Section III, Appendix F, 1989 Edition with no Addenda.

[10] MPR Calculation Number 319-002-01, transmitted by MPR letter H. William McCurdy to JR Hoffman, "Vermont Yankee Seismic Data for Increased Core Flow Evaluation," May 29, 1997.

[11] ANSYS, Releases 6.1 and 8.1, ANSYS, Incorporated, 2002.

[12] GE-NE 0000-0024-7944-3, Vermont Yankee Nuclear Power Station Steam Dryer Modification with Response Spectrum Analysis, June 2004.

[13] "Recommended Weld Quality and Stress Concentration Factors for Use in the Structural Analysis of Exelon Replacement Steam Dryer," GENE Report, e-DRF#0000-0034-6079, February 2005.

Appendix A Vermont Yankee Steam Dryer Differential Pressure

The pressure differentials across the steam dryer are calculated for three categories of events; normal, upset, and faulted conditions. Normal conditions are the steady-state operating conditions. Upset conditions are the anticipated transient events. [[

]] Faulted conditions are the design basis accident events (e.g. main steam line break). The pressure differentials across the steam dryer for the normal conditions at EPU power level are summarized in Table A-1.

Table A-1. Steam Dryer Pressure Differentials for Normal Conditions at EPU

[[		

]]

The pressure differentials across the steam dryer due to forward flow for upset conditions at EPU power level are summarized in Table A-2.

Table A-2. Dryer Delta-P for EPU Forward Flow Upset Conditions

[[	
	]]

The maximum acoustic loads on the dryer face at EPU power level are summarized in Table A-3. Typical pressure time history is shown in Figure A-1.

Table A-3. Maximum TSV Acoustic Load on the Dryer Face at EPU

[[						

]]

[[

]]

Figure A-1. Typical TSV Load Time Histories

Appendix B Acoustic Pressure Stress Intensity Contour Plots

[[

]]

[[

]]

Figure B-1 Inner hood base plate

[[

]]

Figure B-2a Modified outer cover plate, includes tips

[[

]]

Figure B-2b Modified outer cover plate, exclude tips

[[

]]

Figure B-3a Original top hood (all hood)

[[

]]

Figure B-3b Modified top hood (outer hood)

[[

]]

Figure B-3c Hood top plates (inner hood)

[[

]]

Figure B-4a Original outer hood, strips

[[

]]

Figure B-4b Modified outer hood, top weld

[[

]]

Figure B-4c Modified outer hood, bottom weld

[[

]]

Figure B-5 Hood vertical plates (inner hood)

[[

]]

Figure B-6 Hood end plates (inner hood)

[[

]]

Figure B-7 Hood end plates (outer hood)

[[

]]

Figure B-8 Inner hood brackets (gussets)

[[

]]

Figure B-9 Steam 'dam'

[[

]]

Figure B-10 Steam 'dam' gussets

[[

]]

Figure B-11 Hood partition plates

[[

]]

Figure B-12 Baffle plates

[[

]]

Figure B-13 Outlet plenum ends

[[

]]

Figure B-14 Dryer support ring

[[

]]

Figure B-15 Bottom cross beams

[[

]]

Figure B-16 Cross beam gussets

[[

]]

Figure B-17a New gusset on cover plate and front hood

[[

]]

Figure B-17b Gusset foot weld to cover plate

[[

]]

Figure B-18 Outer hood, bottom weld

[[

]]

Figure B-19 Cover plate

Attachment 7

Vermont Yankee Nuclear Power Station

Proposed Technical Specification Change No. 263 – Supplement No. 26

Extended Power Uprate

Steam Dryer Analyses and Monitoring

Technical Memorandum No. 05-06, Analysis of Steam Dryer Differential Pressure Loads at Vermont Yankee

Total number of pages in Attachment 7 (excluding this cover sheet) is 45.

C.D.I. Technical Memorandum No. 05-06

Analysis of Steam Dryer Differential Pressure Loads at Vermont Yankee

Revision 1

Prepared by

Continuum Dynamics, Inc.
34 Lexington Avenue
Ewing, NJ 08618

Prepared under PO No. 4500531980 / 07/02/2004 for

Entergy Nuclear Vermont Yankee LLC
320 Governor Hunt Road
Vernon, VT 05354

Approved by

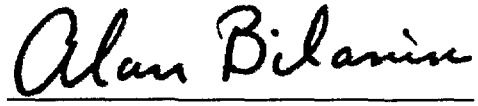

Alan J. Bilanin

March 2005

SUMMARY

A previous report [1] detailed the development of the acoustic circuit analysis on the Vermont Yankee (VY) instrument lines. That analysis corrected the venturi instrument line data by a validated acoustic circuit technique [2] that includes all of the branch lines and Rosemount transmitters on the instrument lines, from the main steam lines to the pressure measurement instruments. These corrected data are then coupled with the strain gage data collected on the main steam lines to predict the differential pressure loads anticipated on the steam dryer. The technical approach for the acoustic circuit analysis of the instrument lines, main steam lines, and steam dome is summarized in [3]. Here the application of these techniques to the Vermont Yankee plant is presented.

MODELING CONSIDERATIONS

The VY steam supply system is broken into two distinct analyses: a Helmholtz solution within the steam dome and an acoustic circuit analysis in the main steam lines.

In the Helmholtz analysis the complex three-dimensional geometry of the steam dryer and steam dome are rendered onto a uniformly-spaced rectangular grid (with mesh spacing of 3 inches), and a solution is obtained for the Helmholtz equation

$$\nabla^2 P + \frac{\omega^2}{a^2} P = 0 \qquad (1)$$

where P is the pressure at a grid point, ω is the circular frequency, and a is acoustic speed in steam. This equation is solved for incremental frequencies from 0 to 200 Hz, subject to the boundary conditions

$$\frac{dP}{dn} = 0 \qquad (2a)$$

normal to all solid surfaces (the steam dome wall and interior and exterior surfaces of the dryer),

$$\frac{dP}{dn} \propto \frac{i\omega}{a} P \qquad (2b)$$

normal to the nominal water level surface (steam-water interface), and unit pressure applied to one inlet to a main steam line and zero applied to the other three.

The Helmholtz solution is coupled to an acoustic circuit solution in the main steam lines. The acoustic circuit analysis divides the main steam lines into elements, which are each characterized by length L, cross-sectional area A, fluid mean density $\bar{\rho}$, fluid mean flow velocity $\bar{U}$, and fluid

acoustic speed $\bar{a}$. Application of acoustic circuit methodology generates solutions for the fluctuating pressure P_n and velocity u_n in the n^{th} element of the form

$$P_n = \left[A_n e^{ik_{1n}X_n} + B_n e^{ik_{2n}X_n}\right] e^{i\omega t} \tag{3a}$$

$$u_n = -\frac{1}{\rho \bar{a}^2}\left[\frac{(\omega + \bar{U}_n k_{1n})}{k_{1n}} A_n e^{ik_{1n}X_n} + \frac{(\omega + \bar{U}_n k_{2n})}{k_{2n}} B_n e^{ik_{2n}X_n}\right] e^{i\omega t} \tag{3b}$$

where harmonic time dependence of the form $e^{i\omega t}$ has been assumed. The wave numbers k_{1n} and k_{2n} are the two complex roots of the equation

$$k_n^2 + i\frac{f_n|\bar{U}_n|}{D_n \bar{a}^2}(\omega + \bar{U}_n k_n) - \frac{1}{\bar{a}^2}(\omega + \bar{U}_n k_n)^2 = 0 \tag{4}$$

where f_n is the pipe friction factor for element n, D_n is the hydrodynamic diameter for element n, and $i = \sqrt{-1}$. A_n and B_n are complex constants which are a function of frequency, and are determined by satisfying continuity of pressure and mass conservation at element junctions.

The resulting system is driven by shear layer motions at geometric discontinuities. These geometric discontinuities exist in the steam delivery system where convective velocities are high.

Solution is obtained with eight pieces of data collected at eight separate locations, two on each main steam line. In the case of VY, each main steam line has been instrumented with one strain gage, in addition to the pressure reading at the end of the venturi instrument line. These eight pieces of data uniquely determine the four inlet sources at the entrances to the main steam lines. As may be seen from the above equations, there are eight unknown coefficients (A_n and B_n on each main steam line) that must be determined before the pressure and velocity are known in the main steam lines. These unknown coefficients are uniquely determined (and unique inlet sources are obtained) when eight independent pieces of data are supplied at each power level. Previously [4], only six pieces of data (pressure at the four venturi instrument lines and two water reference legs) and an assumption regarding inlet source phasing had to be made to close the problem. That restriction no longer applies.

INPUT DATA

VY mounted four strain gages on the main steam lines upstream of the SSV/SRVs, four pressure transducers on the main steam lines at the venturi (venturi instrument lines), four upstream of the turbine (turbine instrument lines), one in the steam chest, and one on each of the two water reference legs. These data sets are tabulated in Table 1. Only the four strain gage data and four venturi instrument line pressure data are examined here. The pressure data were taken at the ends of instrument lines whose detailed lengths were verified by VY personnel. Lines were assumed filled with water to the condensing chambers, and the data were corrected for the

instrument line effects of line length, line connectivity and layout geometry, acoustic speed, transmitter compliance, and frictional losses along the line, by correcting the data in frequency space and then reconstructing the time signal at the instrument line location on the main steam line, as explained below.

Venturi pressure data for five power settings (80%, 85%, 90%, 95%, and 100% power) were supplied previously by VY [4]. Strain gage data were acquired independently, but contained a common signal (the venturi pressure in the A main steam line). The pressure data were corrected to accommodate the analysis by resampling the data from 2000 samples per second to the strain gage sample rate of 1024 samples per second, and shifting the pressure data in time by a constant delay that matched the common signal. The pressure data were filtered before resampling to minimize aliasing of the high frequency content in the original data. The time delays were determined by analyzing the common signal in the frequency domain to estimate the phase delay based on spectral analysis methods. The synchronized strain gage offset times are also shown in Table 1.

Table 1: Summary of VY Data Sets

Data Set	Feed Flow (10^6 lbs/hr)	Date/Time	Data Rate (samples/sec)	Power Level (%)	Strain Gage Offset (sec)
--	6.605	07/09 08:36	2000	100.0	0.889
1	6.605	07/09 08:50	2000	100.0	0.404
--	6.605	07/09 08:51	2000	100.0	0.170
--	6.262	07/09 09:59	2000	95.0	0.026
2	6.262	07/09 10:05	2000	95.0	0.750
--	6.262	07/09 10:06	2000	95.0	0.689
--	5.857	07/09 10:18	2000	90.0	1.161
3	5.857	07/09 10:24	2000	90.0	0.196
--	5.857	07/09 10:24	2000	90.0	0.766
--	5.473	07/09 10:37	2000	85.0	0.960
5	5.473	07/09 10:37	2000	85.0	0.444
--	5.473	07/09 10:38	2000	85.0	0.045
--	5.088	07/09 10:39	2000	80.0	0.639
4	5.088	07/09 10:50	2000	80.0	0.462
--	5.088	07/09 10:51	2000	80.0	0.512

These data were smoothly notch filtered to remove signal content (noise) at the recirculation pump vane passage frequency (and its harmonics) and at frequencies corresponding to electrical interference (60, 120, 180 Hz). Second order notch filters were constructed and applied using a forward-backward digital filtering analysis, by processing the input data in both the forward and reverse directions, and resulting in fourth-order attenuation and no phase delay. The resulting time sequence has precisely zero-phase distortion and double the filter order. The filter stopband was 1 Hz.

Sixteen seconds of data were analyzed at each power setting, centered on the second set of 20 seconds of data supplied, and resulting in 16384 samples with a time increment of 0.0009765625 sec. A Fast Fourier transform [5] was used for both the transform and its inverse. To present a clear picture of the frequency effects, the PSD sampling size was reduced to 1024 samples with a 50% overlap window [5]. The effects of these operations may be seen in the figures presented later in this report.

COMPLIANCE EFFECTS

Transfer of the venturi pressure data from the instrument line reading to the main steam lines requires the application of an acoustic circuit model to the instrument line geometry shown schematically in Figure 1. This circuit required an analysis of the response of the Rosemount transmitters, located at the ends of every branch on every instrument line. The transmitters are modeled by a spring-mass-damper system, thereby permitting the development of a pressure-velocity boundary condition that represents the compliance (and damping) effect of the transmitter on the instrument line.

The compliance modeling begins with the equation

$$AP = M\ddot{x} + c\dot{x} + kx \tag{5}$$

where A is the cross-sectional area of the transmitter, P is the pressure against the transmitter, M is the apparent mass of the transmitter, c is the damping of the transmitter, k is the effective spring constant of the transmitter, x is the displacement of the transmitter diaphragm, $\dot{x}$ is the velocity of the transmitter diaphragm, and $\ddot{x}$ is the acceleration of the transmitter diaphragm. The apparent mass of the transmitter may be defined as

$$M = \rho_f AL + \rho_d At \tag{6}$$

where ρ_f is the density of the fluid, ρ_d is the density of the diaphragm, L is the depth of the fluid, and t is the thickness of the diaphragm. It can also be seen that conservation of mass requires

$$\dot{x}A = uA_i \tag{7}$$

where A_i is the cross-sectional area of the inlet pipe to the transmitter. The governing equation is transformed to frequency space with the two substitutions

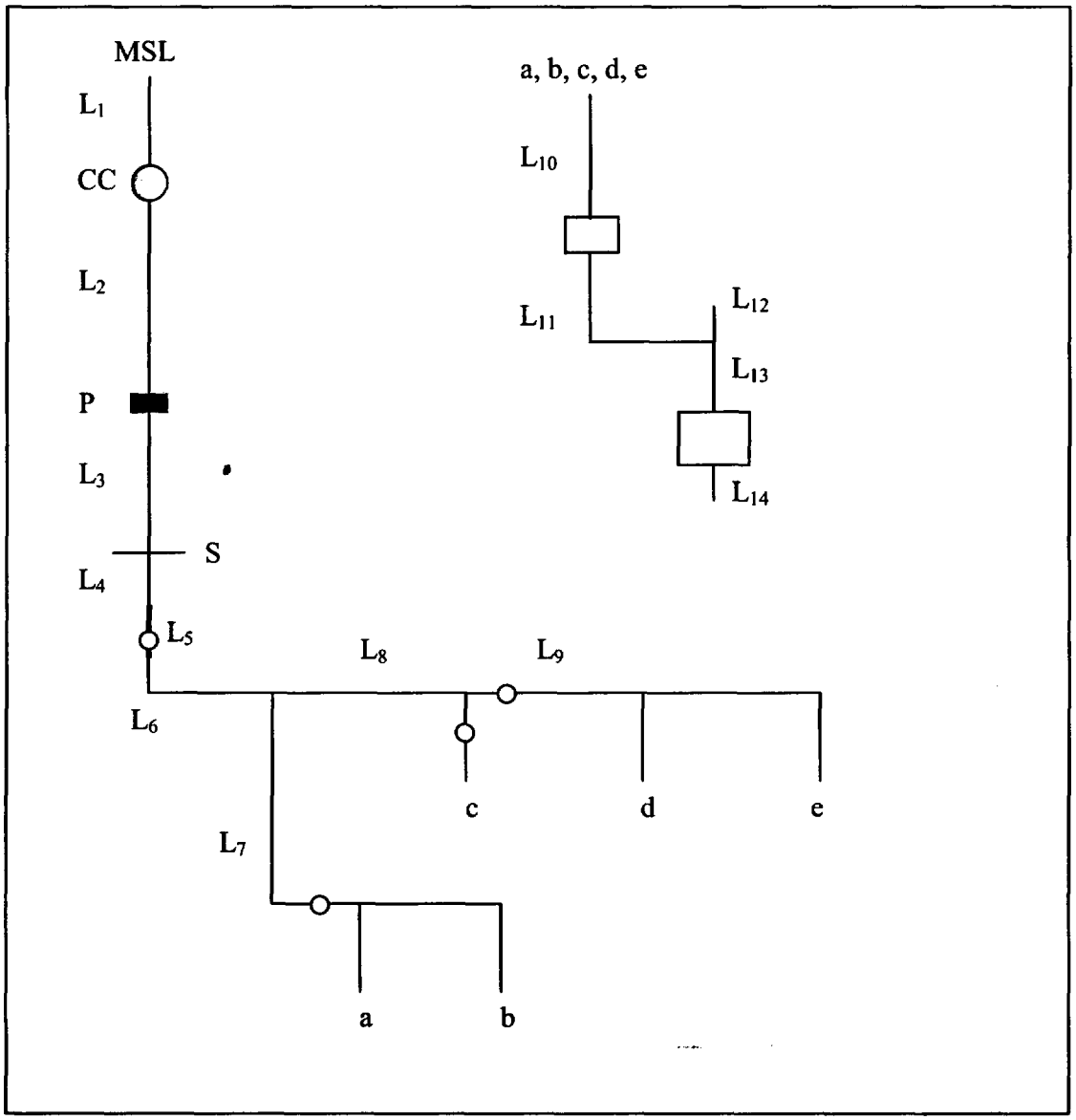

Figure 1. Schematic of typical VY venturi instrument line. The notation is MSL = Main Steam Line, CC = Condensing Chamber, P = Penetration, Gray Box = Whitey Valve Manifold (on lines a, b, d, and e) and Dragon Manifold (on line c), Empty Box = Rosemount Transmitter (on line c: positioned with empty box – not shown – off L_{12}, with empty box off L_{13} representing the Sensotec FP2000 pressure measuring instrument), Open Circle = Valve, S = Location where detailed instrument line sketch begins.

$$\ddot{x} = i\omega\dot{x} \tag{8a}$$

$$x = \frac{\dot{x}}{i\omega} \tag{8b}$$

The effective spring constant can be represented by the transmitter compliance K

$$K = \frac{\Delta V}{\Delta P} = \frac{A\Delta x}{\Delta P}$$

which gives

$$k = \frac{A^2}{K} \tag{9}$$

Substituting these expressions into Equation 5 gives the equation

$$P = \left((\rho_f L + \rho_d t) i\omega \frac{A_i}{A} + \frac{cA_i}{A^2} + \frac{A_i}{i\omega K} \right) u \tag{10}$$

Dividing both sides of the equation by ρa^2 gives an equation relating

$$\hat{P} = \frac{P}{\rho a^2}$$

$$\hat{u} = \frac{u}{a}$$

which is

$$\hat{P} = \left(\frac{(\rho_f L + \rho_d t) i\omega}{\rho a} \frac{A_i}{A} + \frac{cA_i}{\rho a A^2} + \frac{A_i}{i\omega K \rho a} \right) \hat{u} \tag{11}$$

By defining

$$\overline{K} = \frac{K\rho a}{A_i}$$

$$\overline{M} = \frac{\rho_f L + \rho_d t}{\rho a}$$

$$\overline{c} = \frac{cA_j}{\rho a A^2}$$

and multiplying through by $i\omega\overline{K}$, the equation becomes

$$i\omega\overline{K}\hat{P} = \left(1 + i\omega\overline{K}\overline{c} - \omega^2\overline{KM}\frac{A_i}{A}\right)\hat{u} \qquad (12)$$

This equation represents the effect of each Rosemount transmitter in the acoustic circuit model of the instrument lines at VY. The physical inputs for the transmitter were supplied by Rosemount from either their catalogue, email, or telephone conversation. The damping parameter was developed from the solution for oscillating flow through a pipe [6].

TRANSFER FUNCTIONS

To test the effects of compliance on the four instrument lines, a sensitivity study was undertaken by varying the amount of compliance in the Rosemount transmitters. In this study the Sensotec compliance was always set at 1 x 10^{-7} in^3/psid (its default value), with little change seen between the no compliance case and the no compliance case with the Sensotec compliance turned on. The results are presented in Figure 2. Here the transfer function magnitude $H(\omega)$ is defined such that

$$|T(\omega)| = H(\omega)|S(\omega)|$$

where $T(\omega)$ is the fast Fourier transform coefficient of pressure recorded at the pressure measurement device and $S(\omega)$ is the fast Fourier transform coefficient of pressure at the main steam line. It may be seen that the shape of the transfer functions is a strong function of compliance, as the amplitude changes an order of magnitude from no compliance to 100% compliance. The transfer function is complex and includes phase as well as magnitude. Based on the sensitivity runs conducted in this report, the dryer loads are primarily influenced by the transfer function amplitude. Therefore the magnitude plots are presented here.

STRAIN GAGE AND CORRECTED PRESSURE DATA

PSDs of the strain gage data (corrected to pressure) are shown in Figure 3 for 100% power and in Figure 4 comparing 100% power with 80% and 90% power. The notch frequencies are accentuated by the 1 Hz bin size Log PSD plots. The filtering used was optimized to eliminate only +/-0.5 Hz at the electrical noise frequencies. This filtering in fact, slightly increases the 0.01 $Prms^2$/Hz noise floor. Therefore this filtering resulted in negligible reduction of calculated dryer load. The comparison in Figure 3 suggests little difference in driving pressure across the power settings supplied for analysis by VY.

For the most part, above 50 Hz, the strain gage data are at or below their noise floor. It appears that the primary loading of the VY dryer will result from loads which have frequency content below 50 Hz.

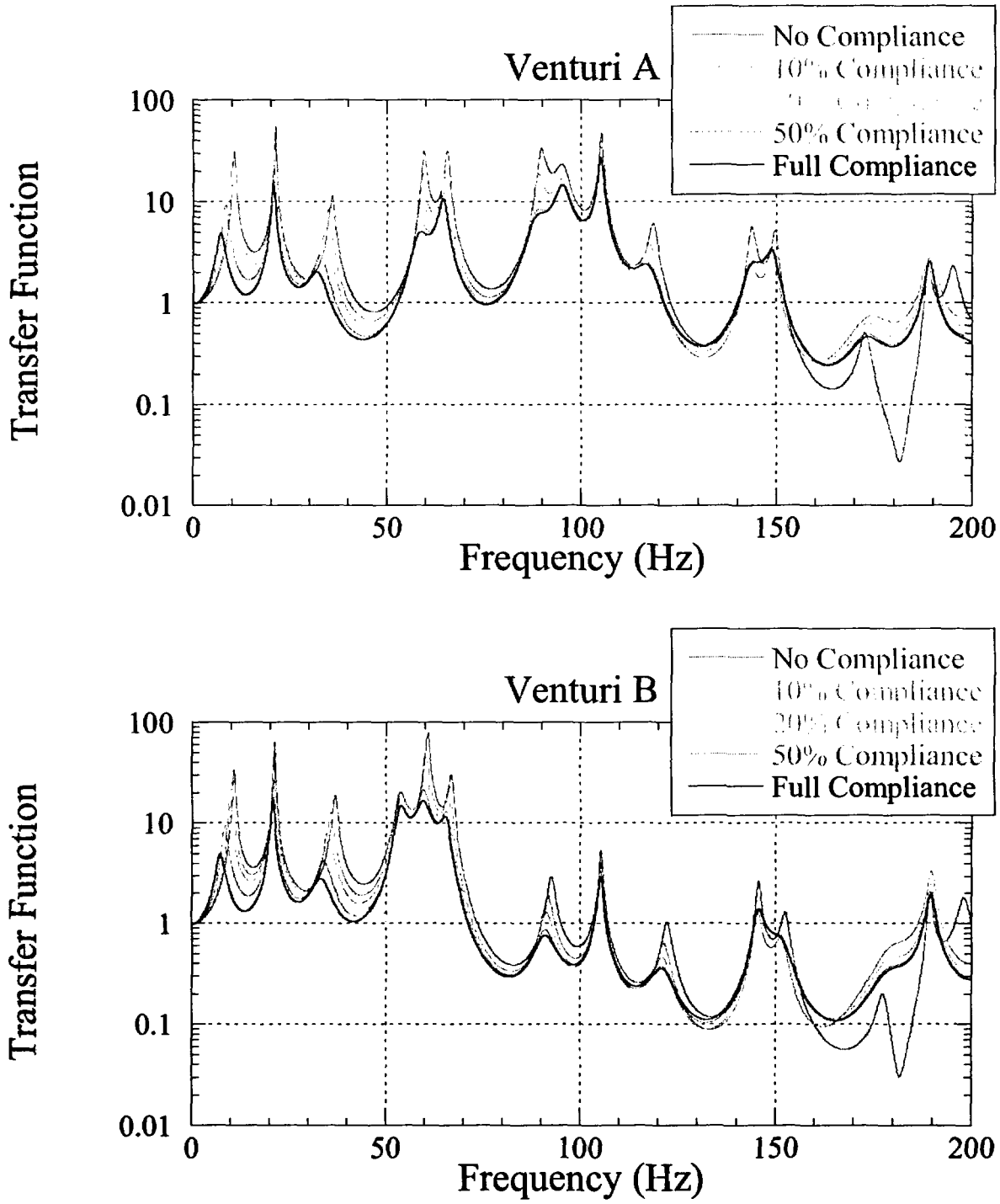

Figure 2a. Transfer function magnitude H(ω) for venturi A (top) and venturi B (bottom) for several values of Rosemount transmitter compliance.

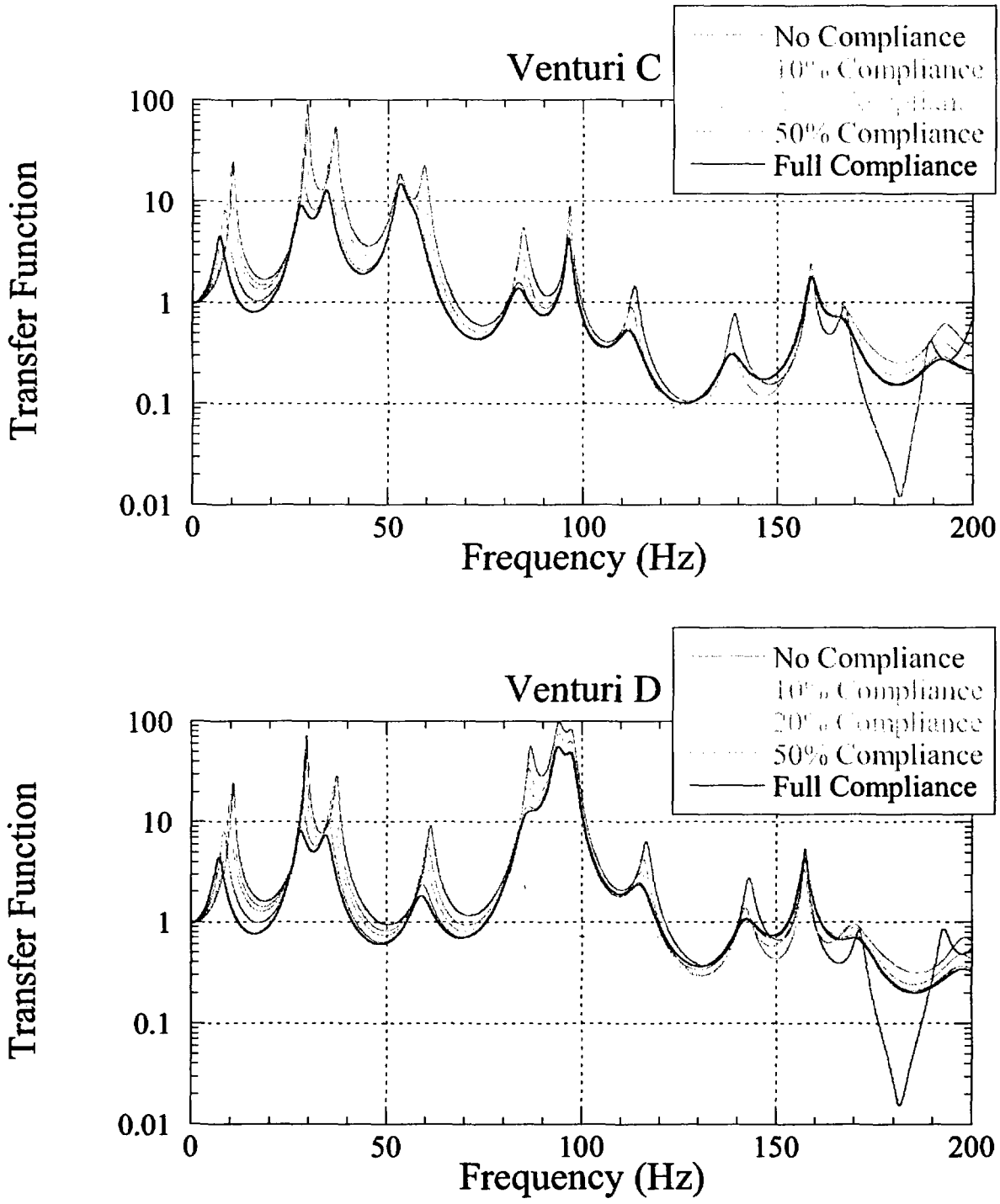

Figure 2b. Transfer function magnitude H(ω) for venturi C (top) and venturi D (bottom) for several values of Rosemount transmitter compliance.

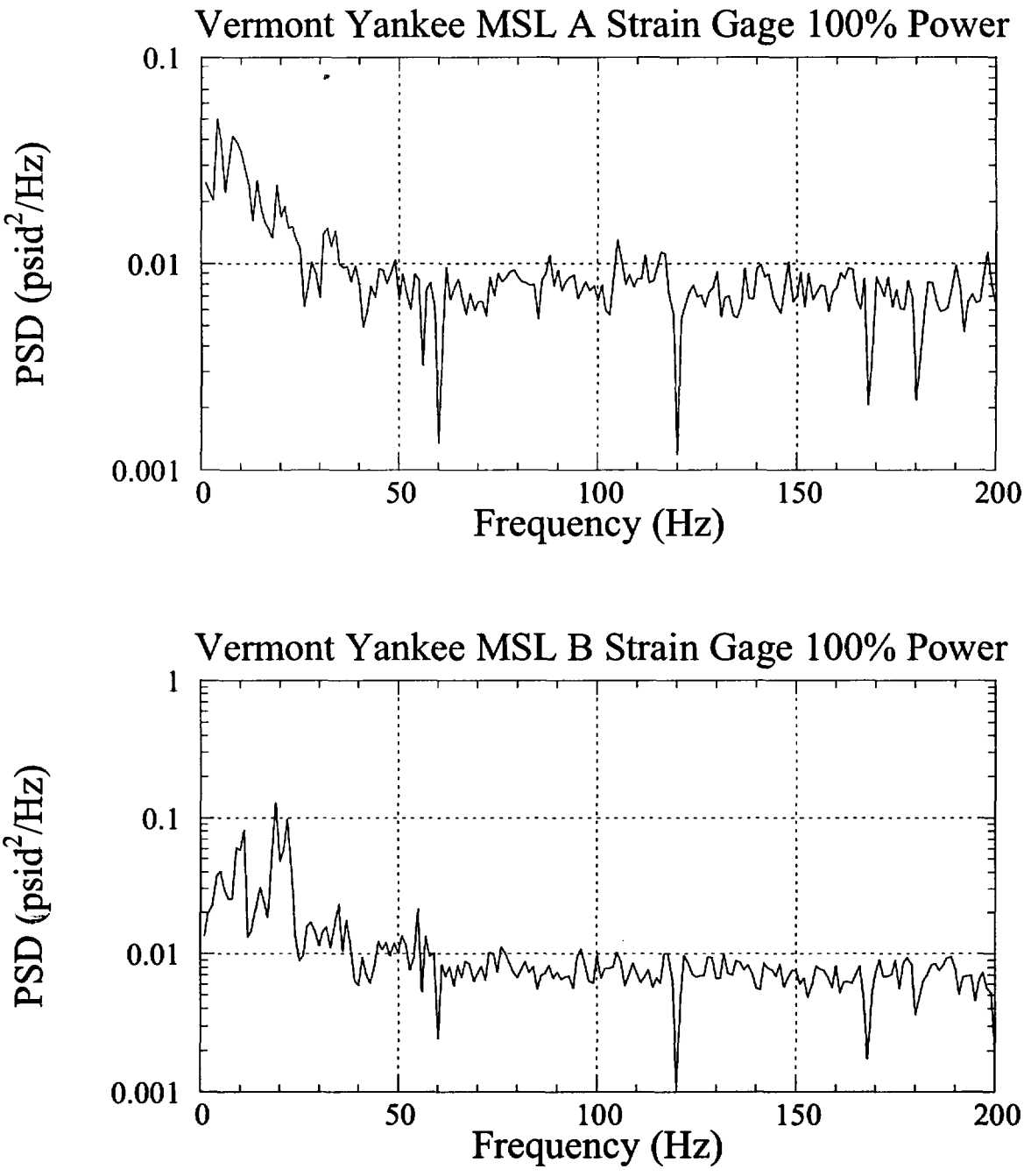

Figure 3a. PSD of filtered strain gage data on the A main steam line (top) and the B main steam line (bottom) for 100% power.

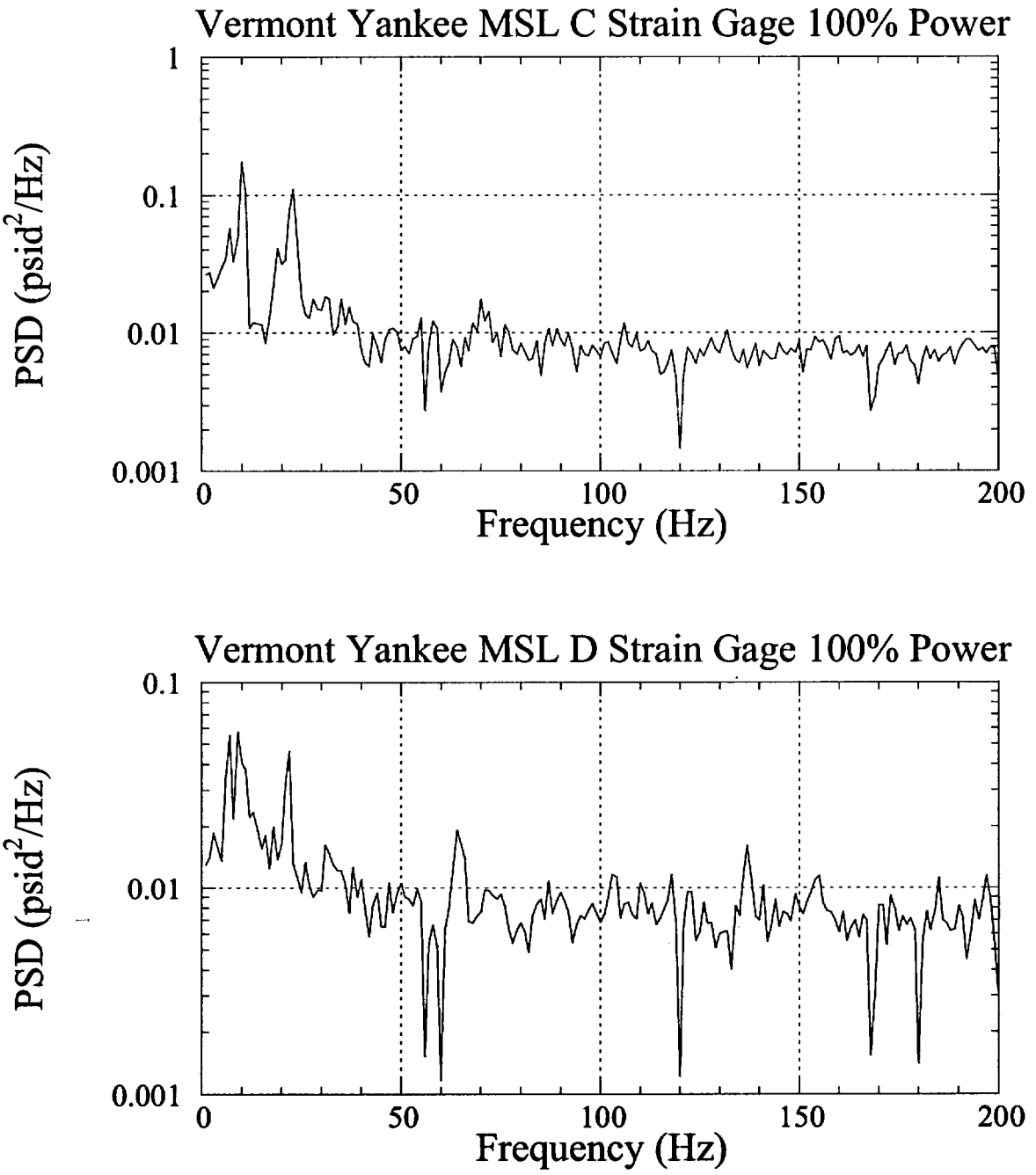

Figure 3b. PSD of filtered strain gage data on the C main steam line (top) and the D main steam line (bottom) for 100% power.

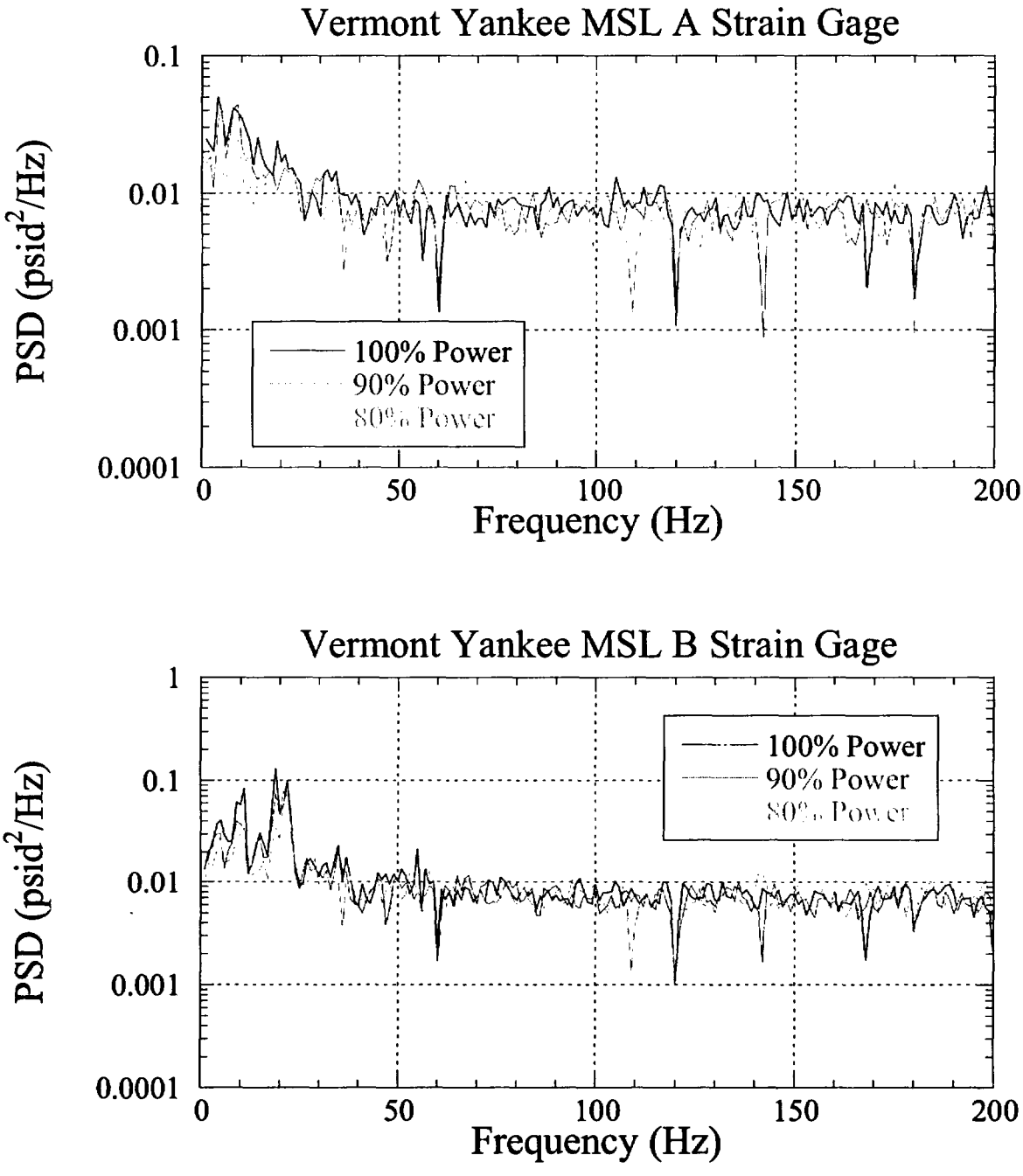

Figure 4a. Comparison of PSD of filtered strain gage data on the A main steam line (top) and the B main steam line (bottom) for 100%, 90%, and 80% power.

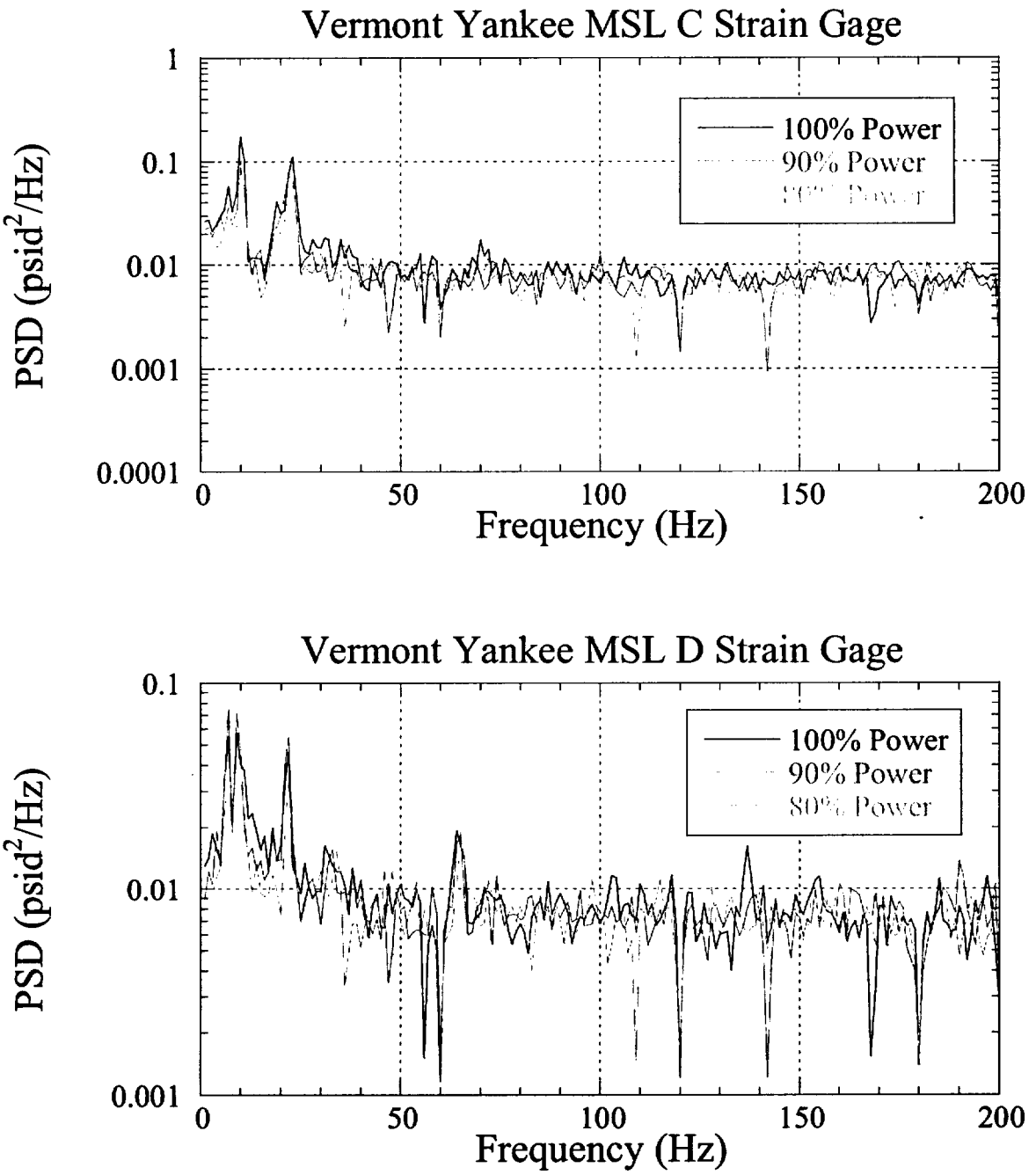

Figure 4b. Comparison of PSD of filtered strain gage data on the C main steam line (top) and the D main steam line (bottom) for 100%, 90%, and 80% power.

PSDs of the corrected venturi pressure data through the instrument lines are shown in Figure 5 for 100% power and in Figure 6 comparing 100% power with 80% and 90% power. The strong similarities between signals across the supplied power settings are clear.

The difference between the venturi pressures and the strain gage equivalent pressures is in the fact that the venturi pressures dip around 50 Hz (for the B and C lines) and 100 Hz (for the A and D lines), and increase with frequency thereafter, whereas the strain gage pressures do not. This behavior suggests that the instrument line correction is adding acoustic energy at higher frequencies, resulting in a conservative signal transferred to the main steam line.

It may be postulated that the pressure recorded at the end of the instrument line is always interpreted as originating from an acoustic wave in the main steam line. In fact, 3D effects such as main steam line turbulence would propagate an acoustic signal down the instrument line that, in this analysis, would be interpreted as acoustic, when in fact it is noise. Therefore, the pressure time histories recorded at the ends of the instrument lines contain both acoustic and turbulent noise. At 100% power, main steam line flow velocities are U = 144 ft/sec, and the largest eddies scale with the main steam line diameter D = 1.34 ft. Therefore, flow noise is anticipated at frequencies above U/D = 100 Hz.

LOW RESOLUTION GRID MESH RESULTS

These data were used to drive an acoustic circuit model of the main steam lines and steam dome, to construct low resolution grid mesh results on the steam dryer geometry illustrated in Figures 7 and 8. The summary results of this effort are shown in Figure 9. Very little difference may be seen in maximum steam dryer loads between power levels, consistent with similar behavior observed in Dresden 2 (DR2). Figure 10 compares the PSD at the peak load point on the low resolution grid (node numbers 98 on the A-B side and 6 on the C-D side) for 100%, 90%, and 80% power. The consistency across power level is maintained in the load predictions as well.

HIGH RESOLUTION GRID MESH RESULTS

A high resolution load result at 100% power was supplied to GE to support the finite element analysis of the VY dryer. This result included time histories at 11,118 nodes located on the dryer, separated by the grid mesh increments illustrated in Figure 8. The loads were delivered separately to GE.

The selected time interval (10.0 to 12.5 seconds) within the 16 seconds examined represents the overall signal content of the entire 16 seconds predicted. This conclusion can be reached by a detailed examination of the peak load prediction on the low resolution grid (node numbers 98 on the A-B side and 6 on the C-D side). The RMS and peak pressure values for the selected 2.5 seconds are 0.0767 and 0.3220 psid, respectively, for the A-B side, and 0.0845 and 0.3010 psid, respectively, for the C-D side, while the RMS and peak pressure values for the entire 16 second time interval are 0.0734 and 0.3365 psid, respectively, for the A-B side, and 0.0794 and 0.3086 psid, respectively, for the C-D side. The time history slice is plotted in Figure 11.

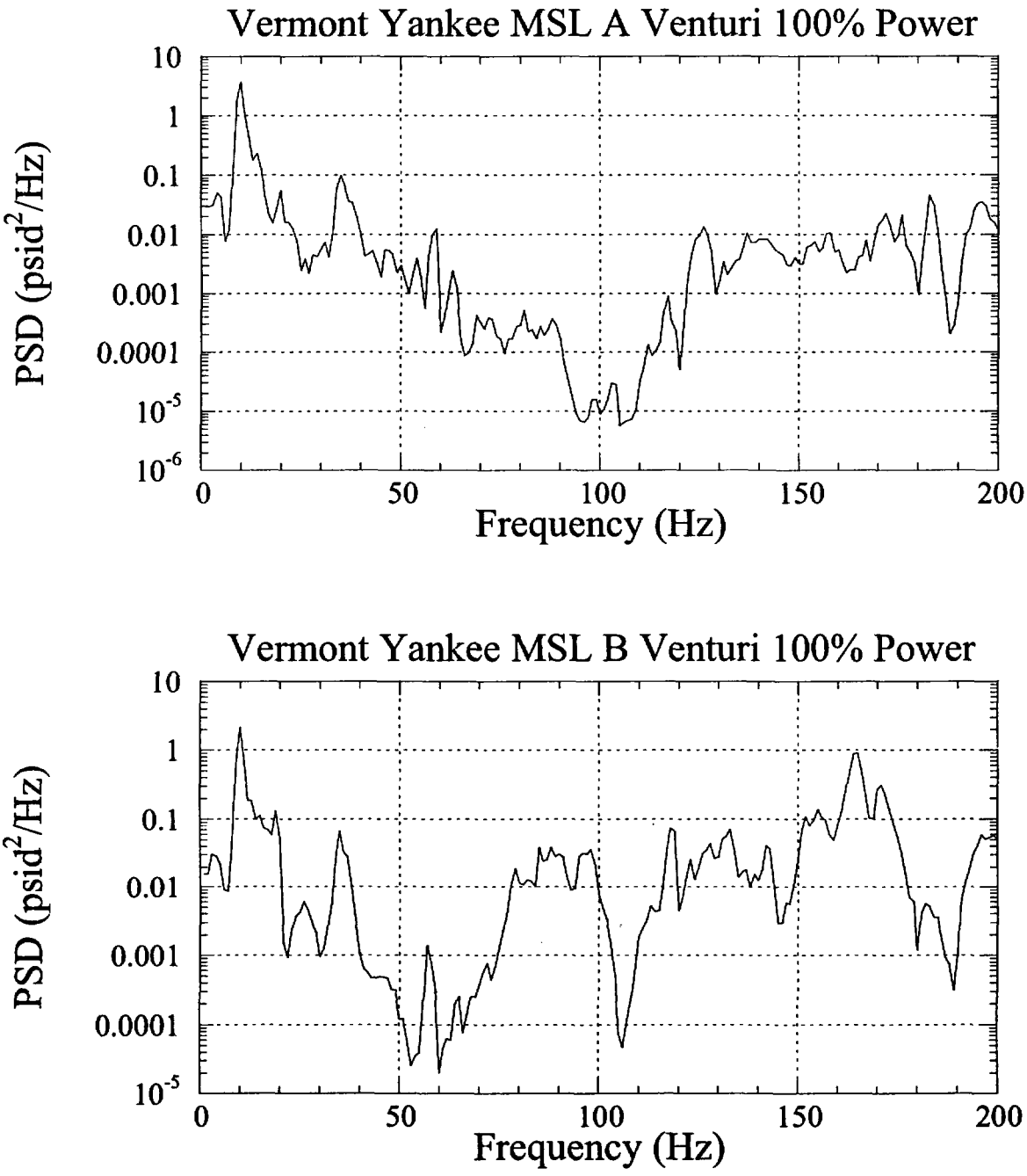

Figure 5a. PSD of instrument line corrected venturi pressure data on the A main steam line (top) and the B main steam line (bottom) for 100% power.

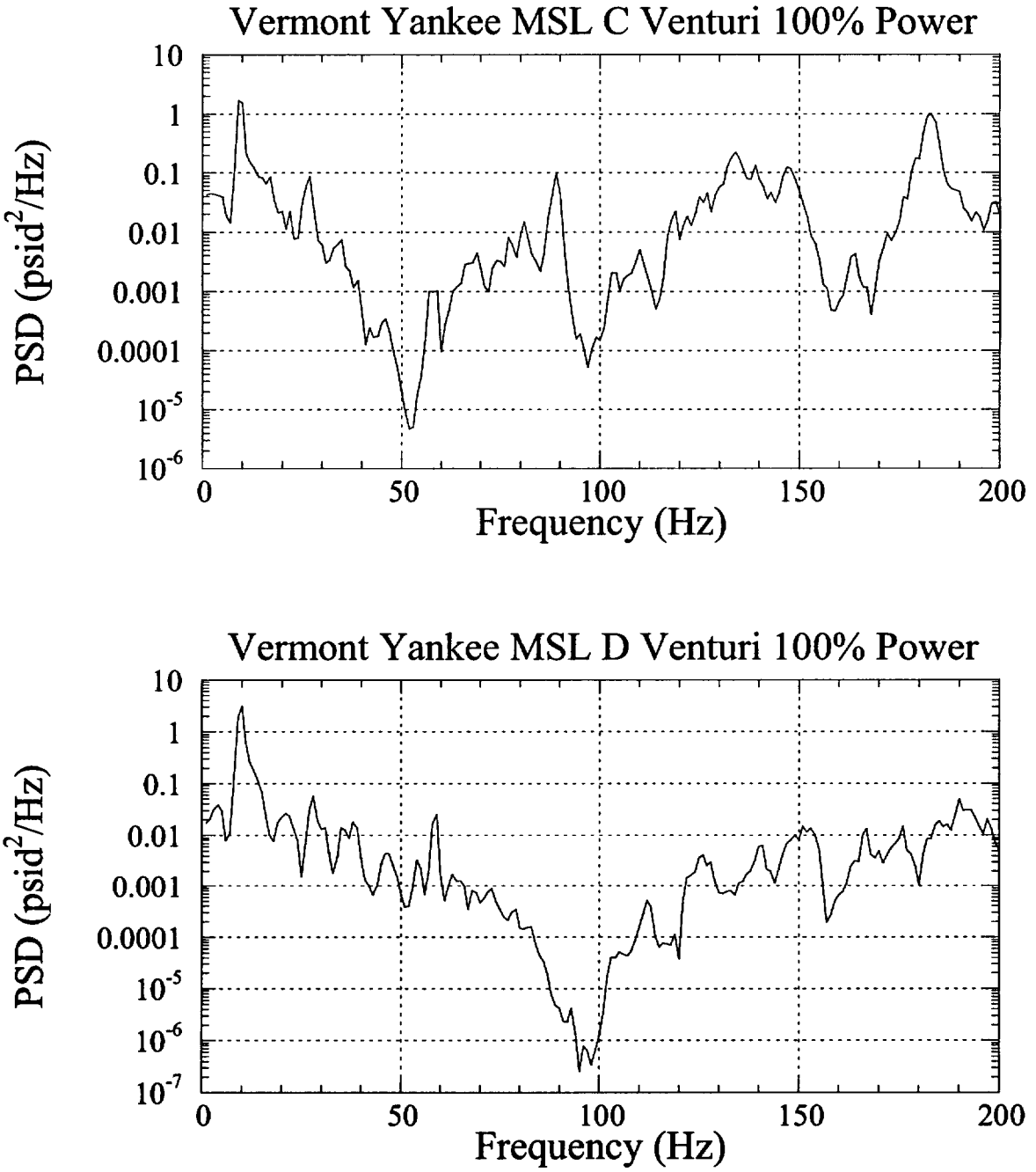

Figure 5b. PSD of instrument line corrected venturi pressure data on the C main steam line (top) and the D main steam line (bottom) for 100% power.

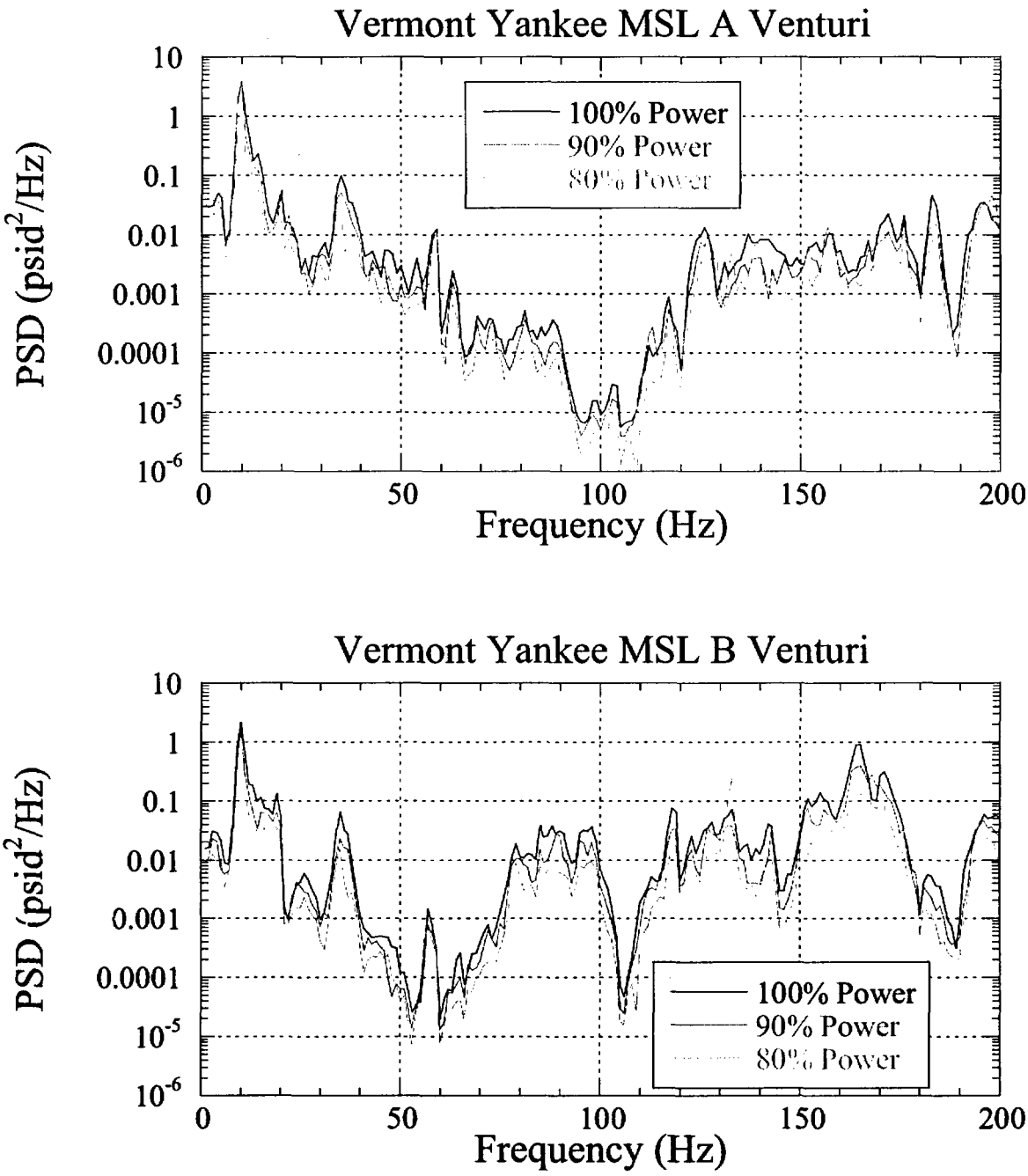

Figure 6a. Comparison of PSD of instrument line corrected venturi pressure data on the A main steam line (top) and the B main steam line (bottom) for 100%, 90%, and 80% power.

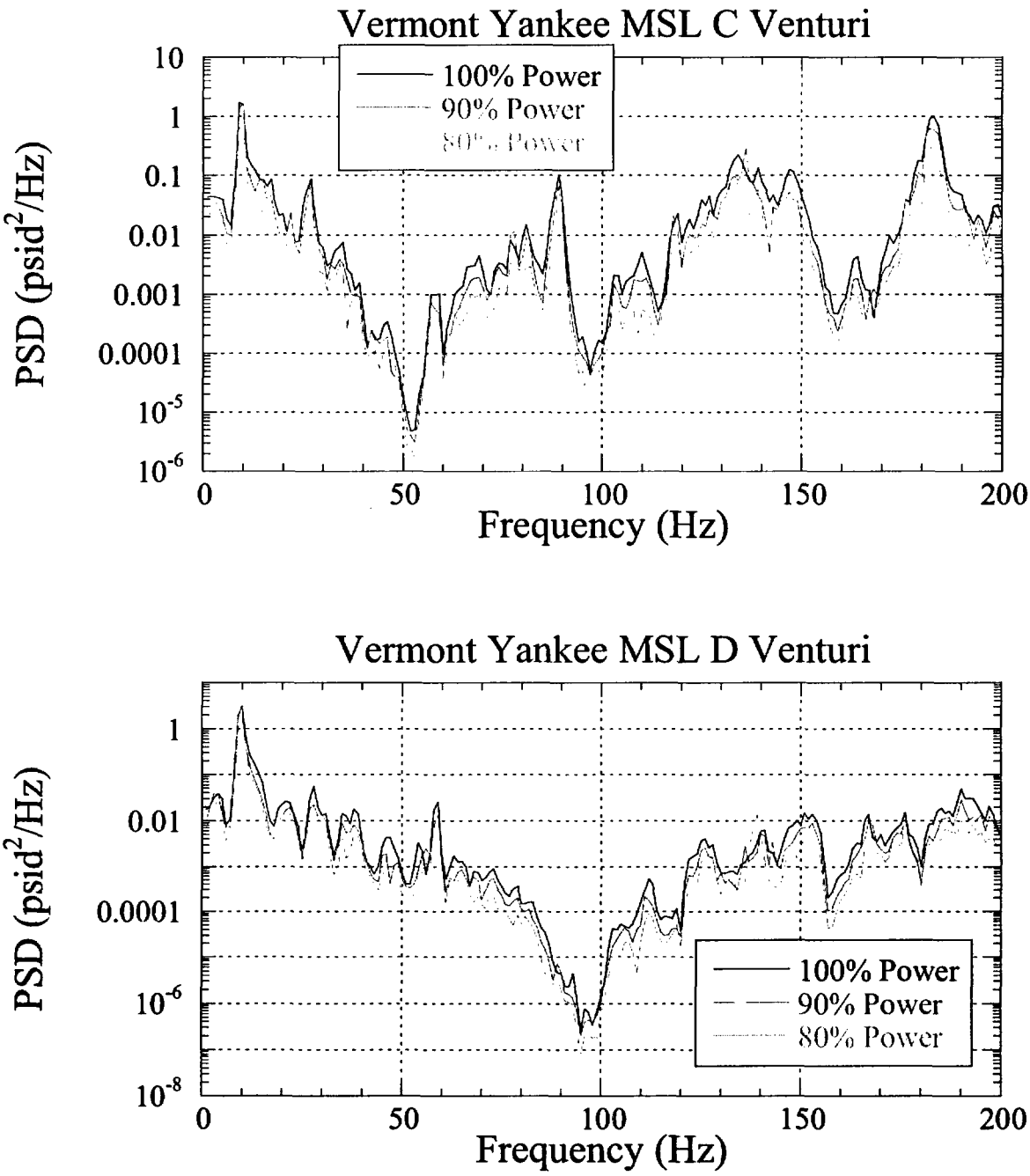

Figure 6b. Comparison of PSD of instrument line corrected venturi pressure data on the C main steam line (top) and the D main steam line (bottom) for 100%, 90%, and 80% power.

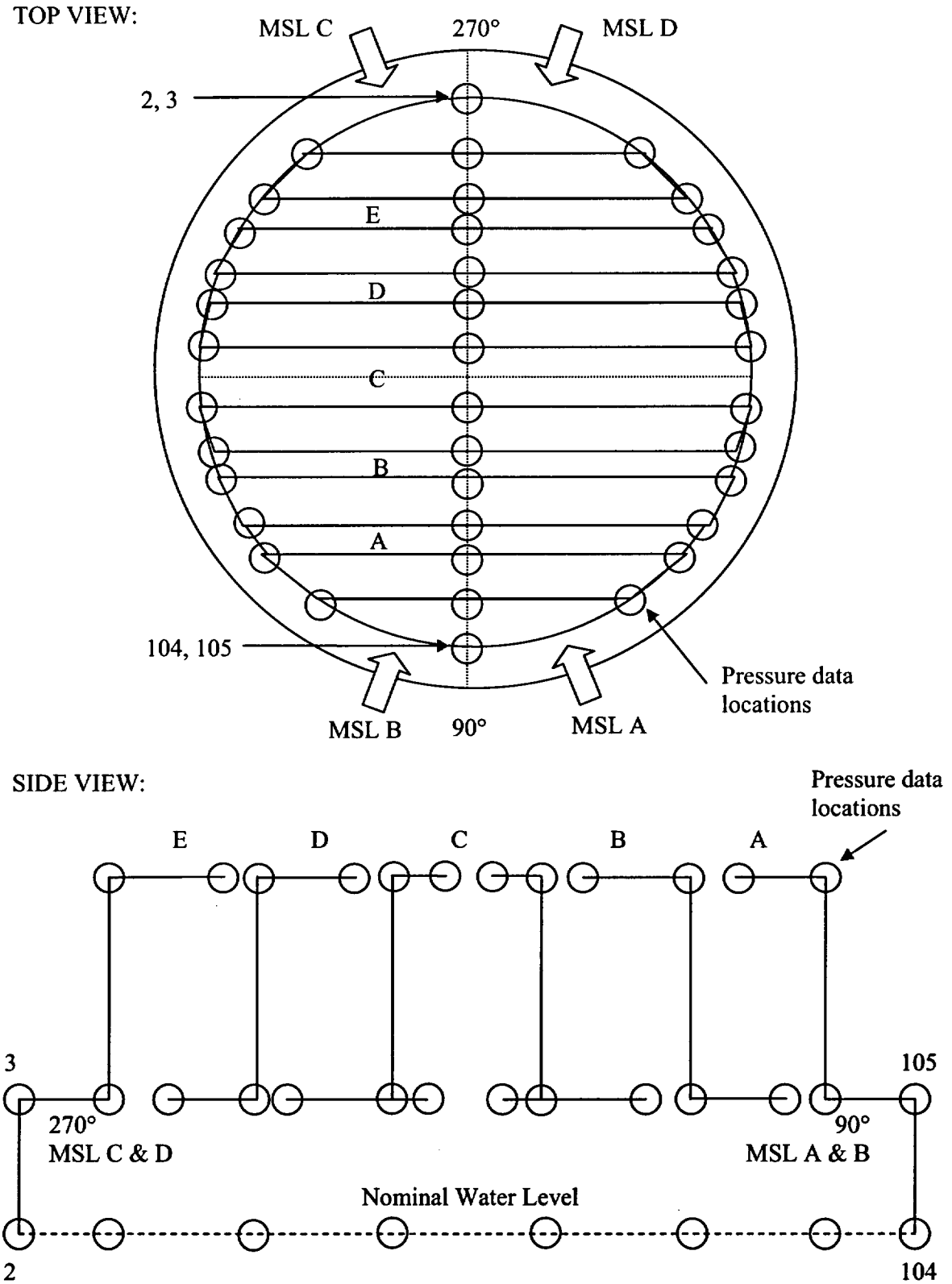

Figure 7. Top and side view schematic of pressure node locations on the VY steam dryer.

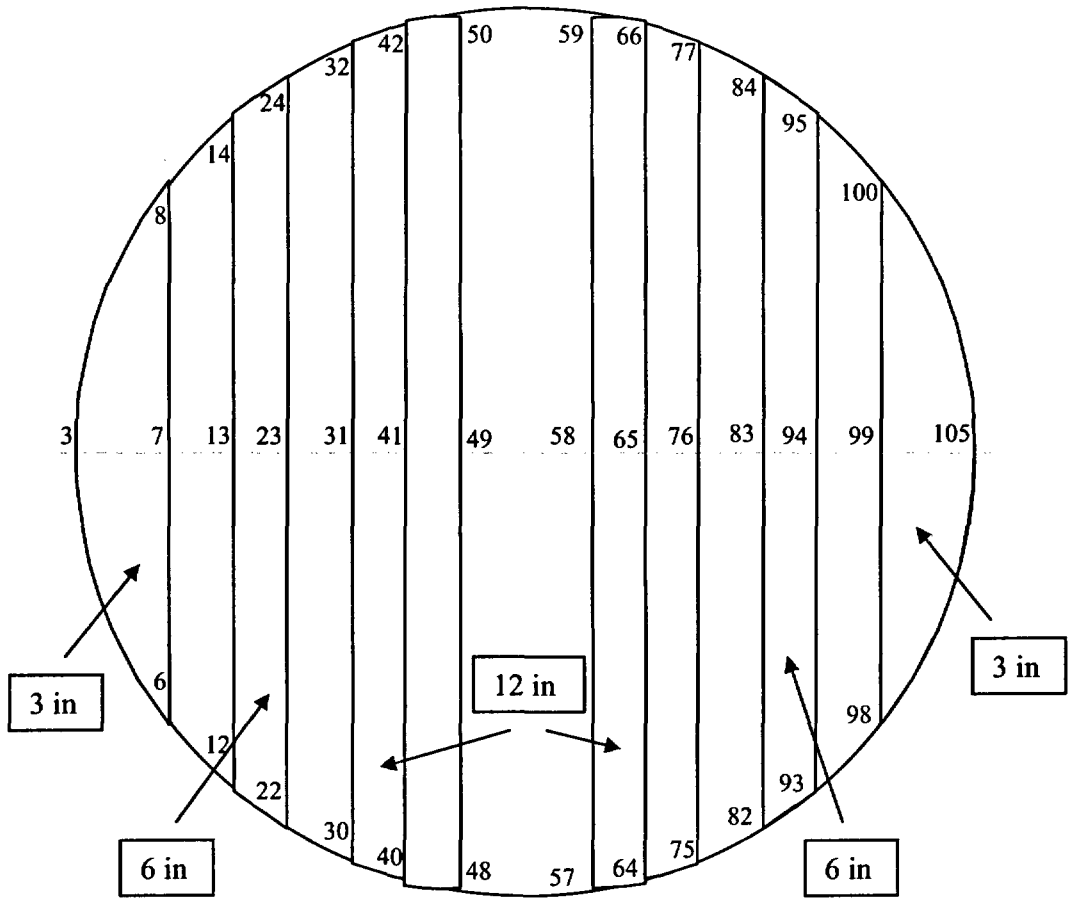

Figure 8a. Bottom plates pressure node locations on the VY dryer, with pressures acting downward in the notation defined here. The high resolution grid mesh is 3 inches on the cover plates, 6 inches on the first bottom plates, and 12 inches on the rest of the bottom plates.

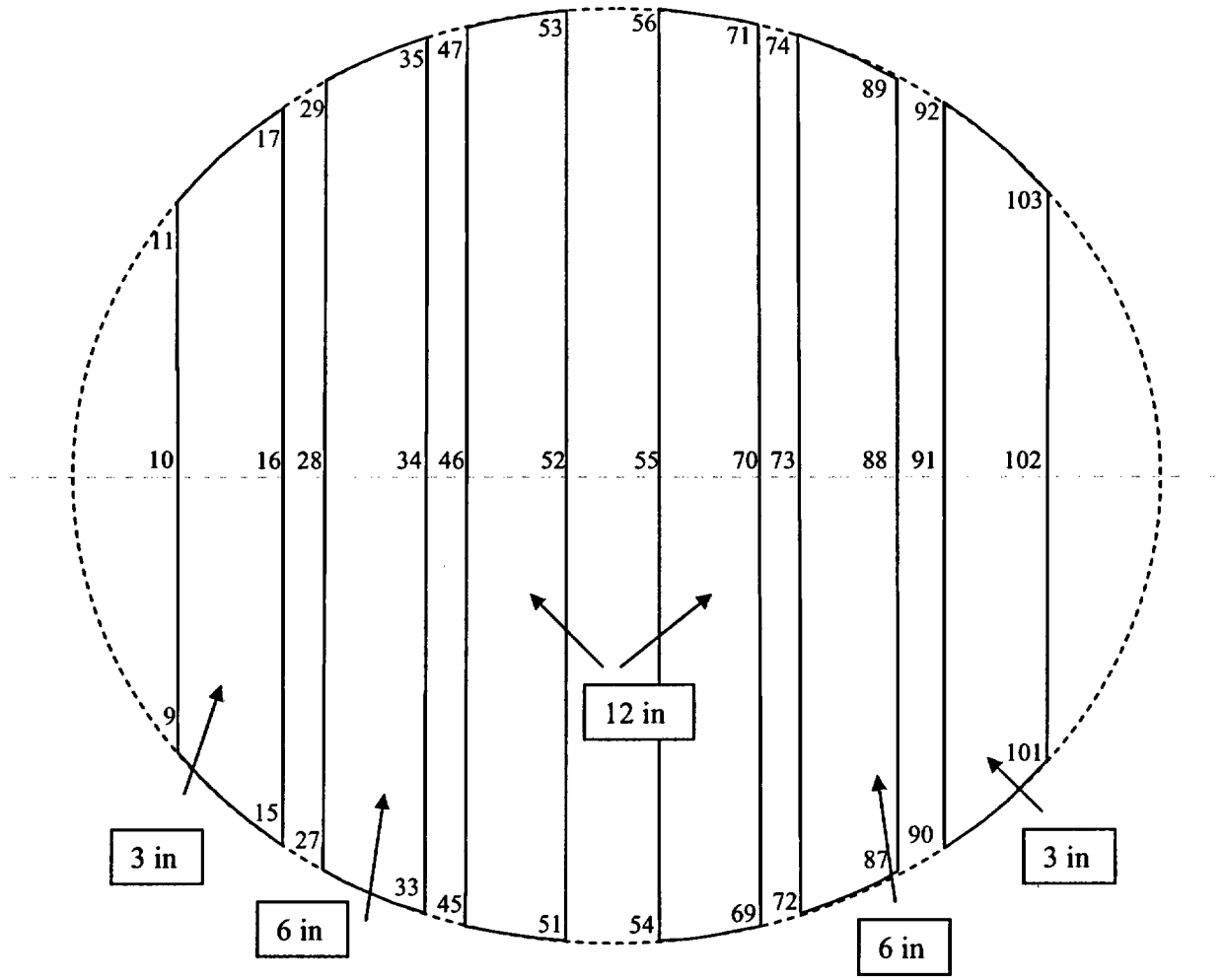

Figure 8b. Upper plates pressure node locations on the VY dryer, with pressures acting downward in the notation defined here. The high resolution grid mesh is 3 inches on the outer top plates, 6 inches on the first inner top plates, and 12 inches on the rest of the inner top plates.

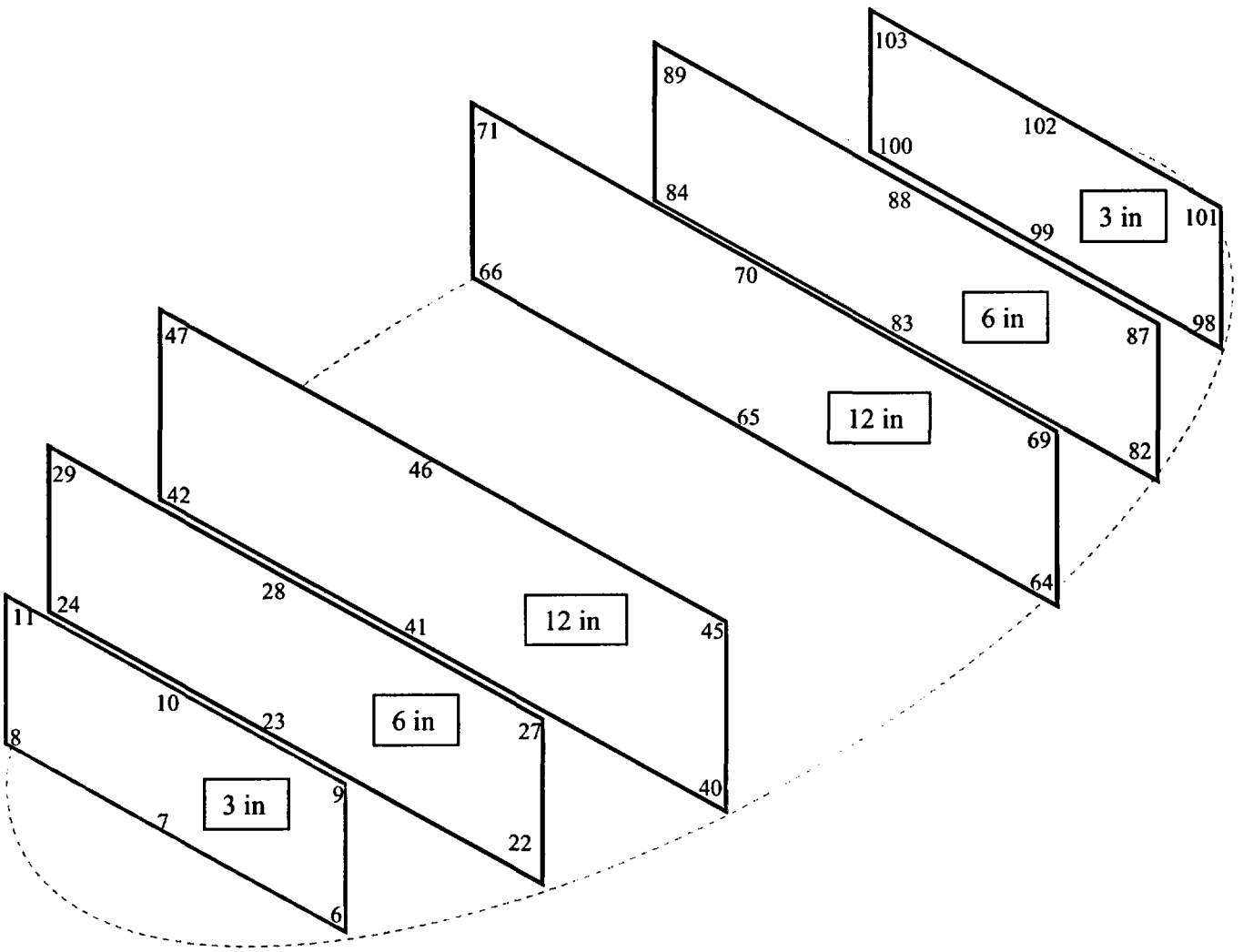

Figure 8c. Vertical plates on the VY dryer: Pressures acting left to right on panels 6-11, 22-29, and 40-47; acting right to left on panels 64-71, 82-89, and 98-103. The high resolution grid mesh is 3 inches on the outer bank hoods, 6 inches on the first inside hoods, and 12 inches on the inside hoods.

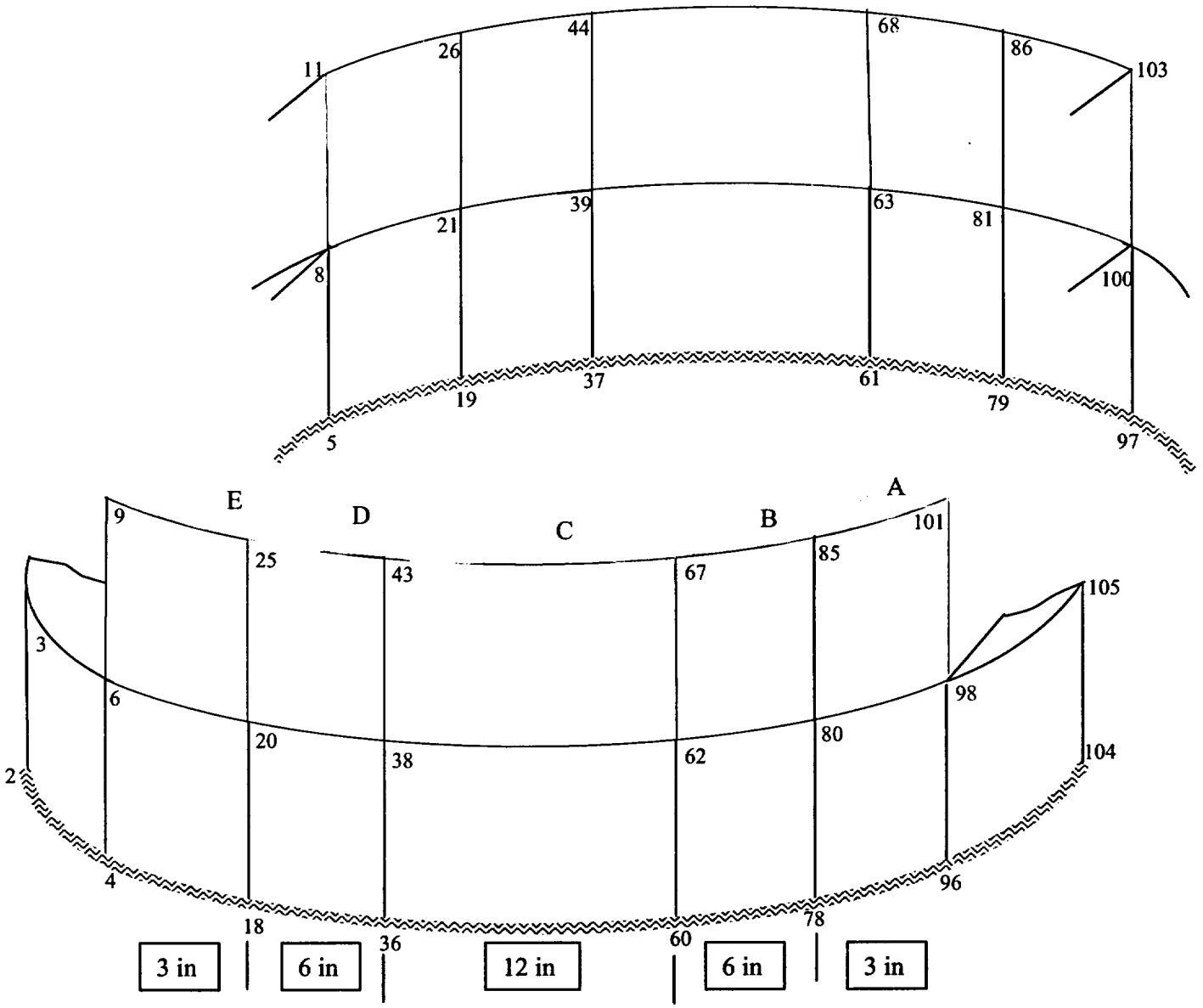

Figure 8d. Skirt plates on the VY dryer: Pressure acting on the outer dryer 0/180 surfaces and the skirt. The high-resolution grid mesh is 3 inches on the outer portion of the skirt closest to the main steam lines, 6 inches on the sections nearer the center of the dryer, and 12 inches on the center of the dryer.

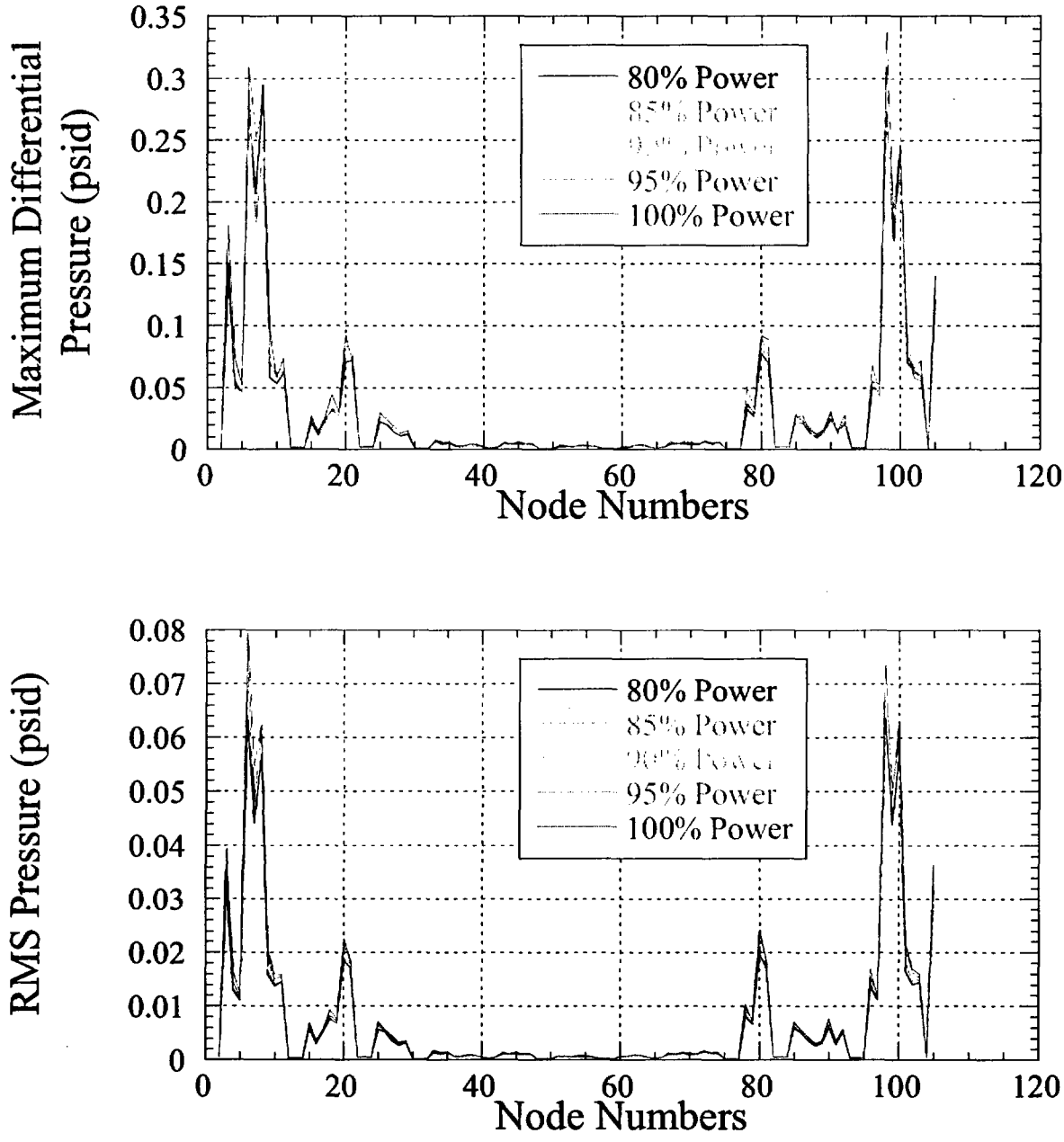

Figure 9. Low resolution grid mesh results for VY for 80% power (black curve), 85% (red curve), 90% power (gray curve), 95% power (green curve), and 100% power (blue curve).

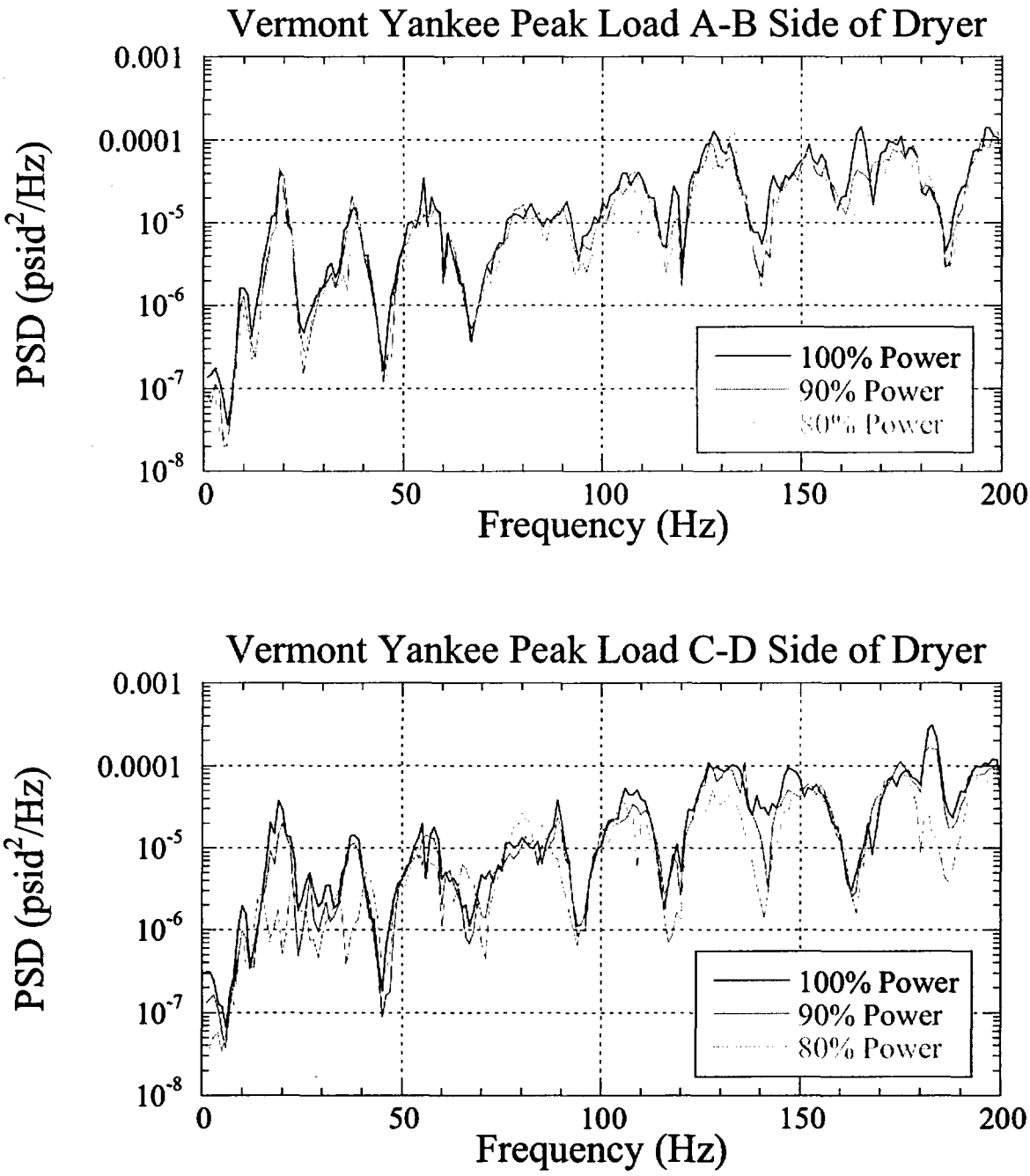

Figure 10. Comparison of PSD at the low resolution dryer locations where peak load is predicted: X on the A-B side (top) and Y on the C-D side (bottom).

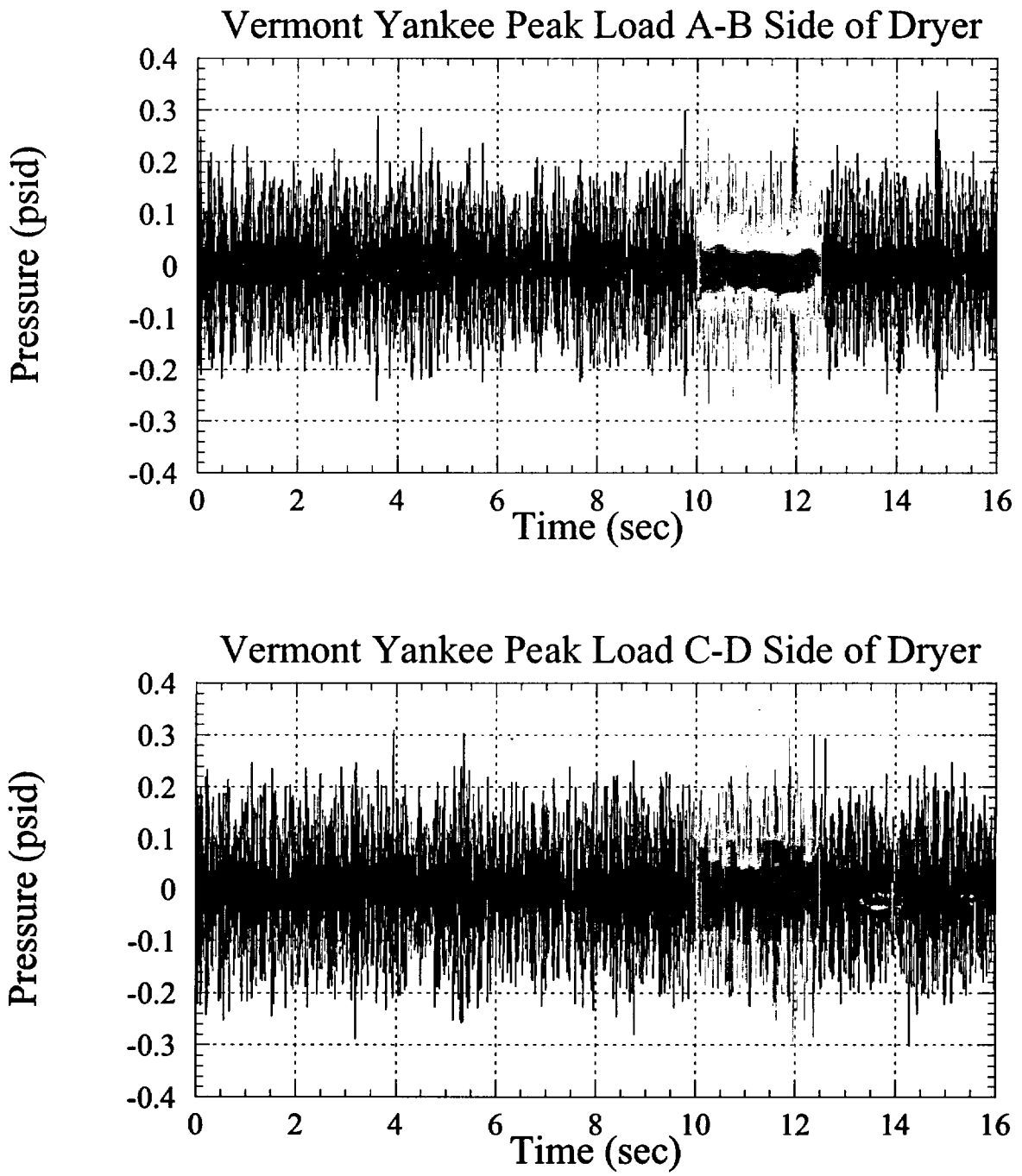

Figure 11. Time slice (in blue) selected for high resolution grid mesh results, compared with the entire time history prediction at 100% power (in black): peak load on the A-B side of the dryer (top); peak load on the C-D side of the dryer (bottom), both based on the low resolution grid mesh results.

The high resolution grid mesh results add additional load definition only approximated by the low resolution grid mesh results, and finds a more accurate prediction of the maximum load amplitude across the VY dryer. For example, the maximum differential pressure load predicted from the low resolution loads is 0.336 psid, while for the high resolution loads it is 0.648 psid.

COMPARISON WITH DRESDEN 2 AND QUAD CITIES 2

Recently, strain gage data were collected at DR2, and low and high resolution load definitions were supplied to Exelon [7]. These strain gage data at OLTP are compared with VY strain gage data at 100% power in Figure 12. The feed flow rate for VY is 6.605 Mlbs/hr (from Table 1), while the feed flow rate for DR2 at OLTP is 9.71 Mlbs/hr. It may be seen that the DR2 strain gage data decrease in magnitude with frequency increase, while the VY data do not. Clearly, the VY noise floor on the strain gages is higher than the DR2 noise floor on their strain gages, effectively increasing the higher frequency energy content of the pressure signal supplied to the steam dryer. Structural Integrity Associates estimates the noise floor at 0.008 $psid^2/Hz$ [8].

The low-resolution grid mesh results for VY may be compared with similar nodal locations on DR2 as shown in Figure 13. Here the nodes associated with the center bank and the top skirt have been removed from the low resolution results previously obtained for DR2 [7], reducing the total number of nodes on these dryers to 104, the same as on VY (and at the same relative locations on the dryer – the VY dryer is smaller than the DR2 dryer, however). It may be seen from Figure 13 that VY at 100% power has maximum pressure loads that are 0.730 of the predicted DR2 load at OLTP, on the C-D side of the dryer (0.3086 psid on VY and 0.4228 psid on DR2), and 0.650 of the predicted DR2 load at OLTP, on the A-B side of the dryer (0.3365 psid on VY and 0.5179 psid on DR2). The average load reduction factor is 0.636 across the 104 nodes in the low resolution result, suggesting that VY dryer loads are reduced considerably from those predicted for the DR2 dryer.

The low-resolution grid mesh results for VY may also be compared with similar nodal locations on Quad Cities 2 (QC2) as shown in Figure 14. Again, the feed flow rate for VY is 6.605 Mlbs/hr, while the feed flow rate for QC2 at OLTP is 9.92 Mlbs/hr. It may be seen that VY at 100% power has a maximum pressure load of 0.3086 psid on the C-D side of the dryer, as opposed to 2.1298 psid in QC2, and 0.3365 psid on the A-B side of the dryer, as compared to 2.6294 psid in QC2. A comparison of peak loads on the dryer is shown in Figure 15.

Peak load behavior is quite different, reflecting the added energy content present in QC2. This content is the result of distinct deterministic mechanisms that exist at the feed flow rates at which the QC2 plant operates. These mechanisms increase the dryer loads, and are simply not excited at the much lower feed flow rates at which the VY plant operates; hence, the difference in frequency content. The QC2 load at 92 and 138 Hz is not present in VY.

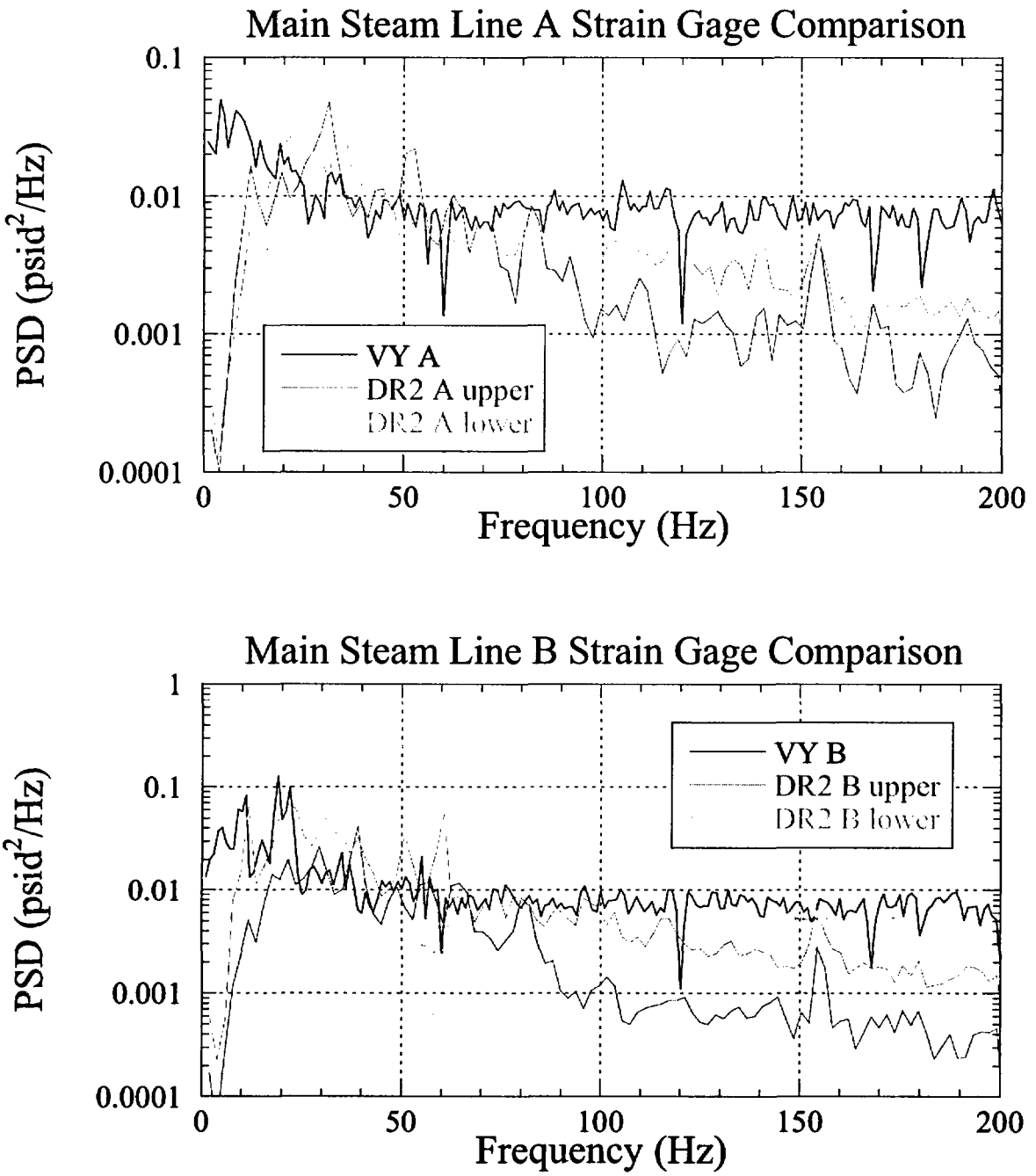

Figure 12a. PSD comparisons of strain gages on VY (black curve), DR2 at their upper locations (blue curve, closer to the steam dome), and DR2 at their lower locations (red curve, farther from the steam dome): main steam line A (top); main steam line B (bottom).

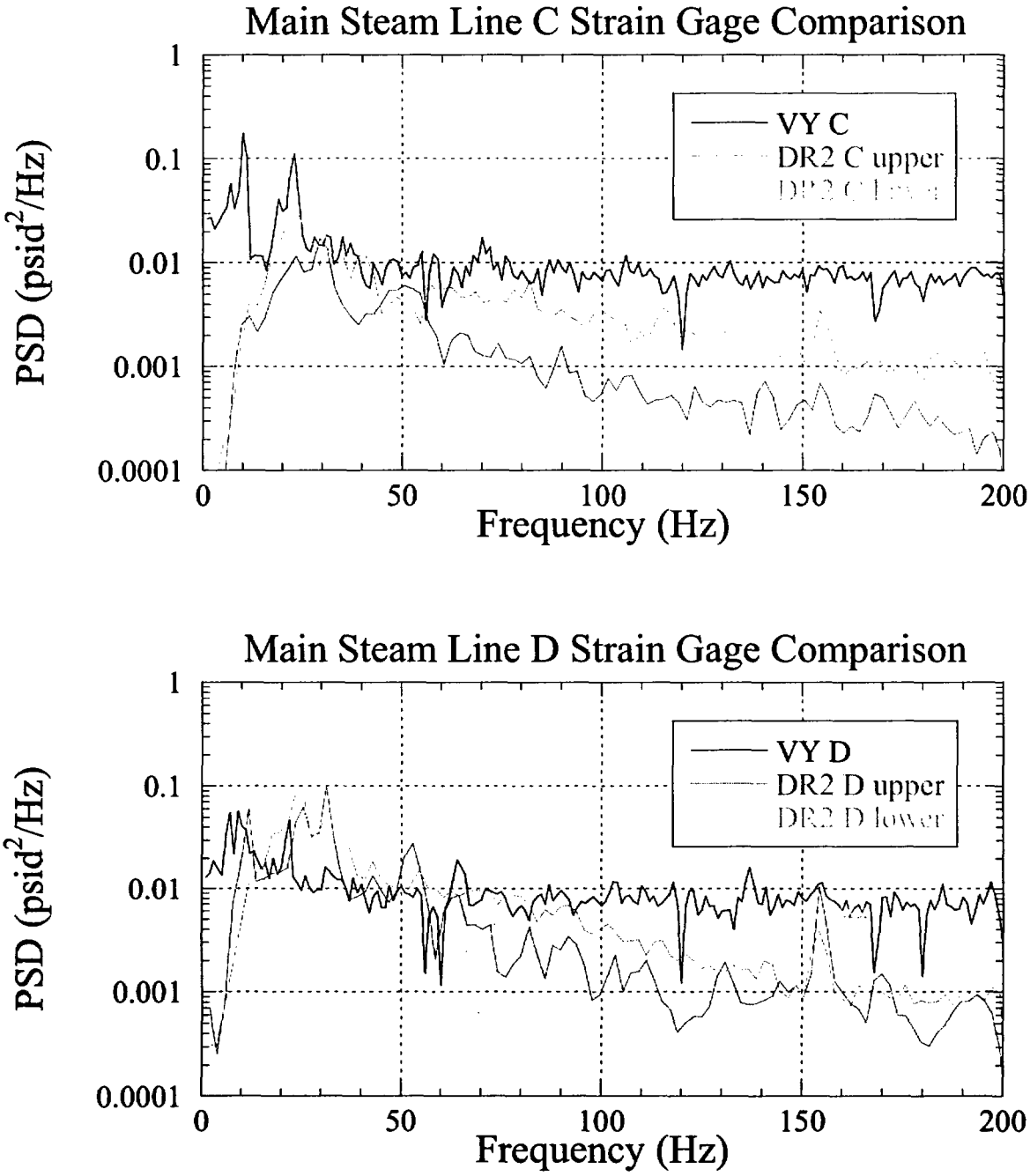

Figure 12b. PSD comparisons of strain gages on VY (black curve), DR2 at their upper locations (blue curve, closer to the steam dome), and DR2 at their lower locations (red curve, farther from the steam dome): main steam line C (top); main steam line D (bottom).

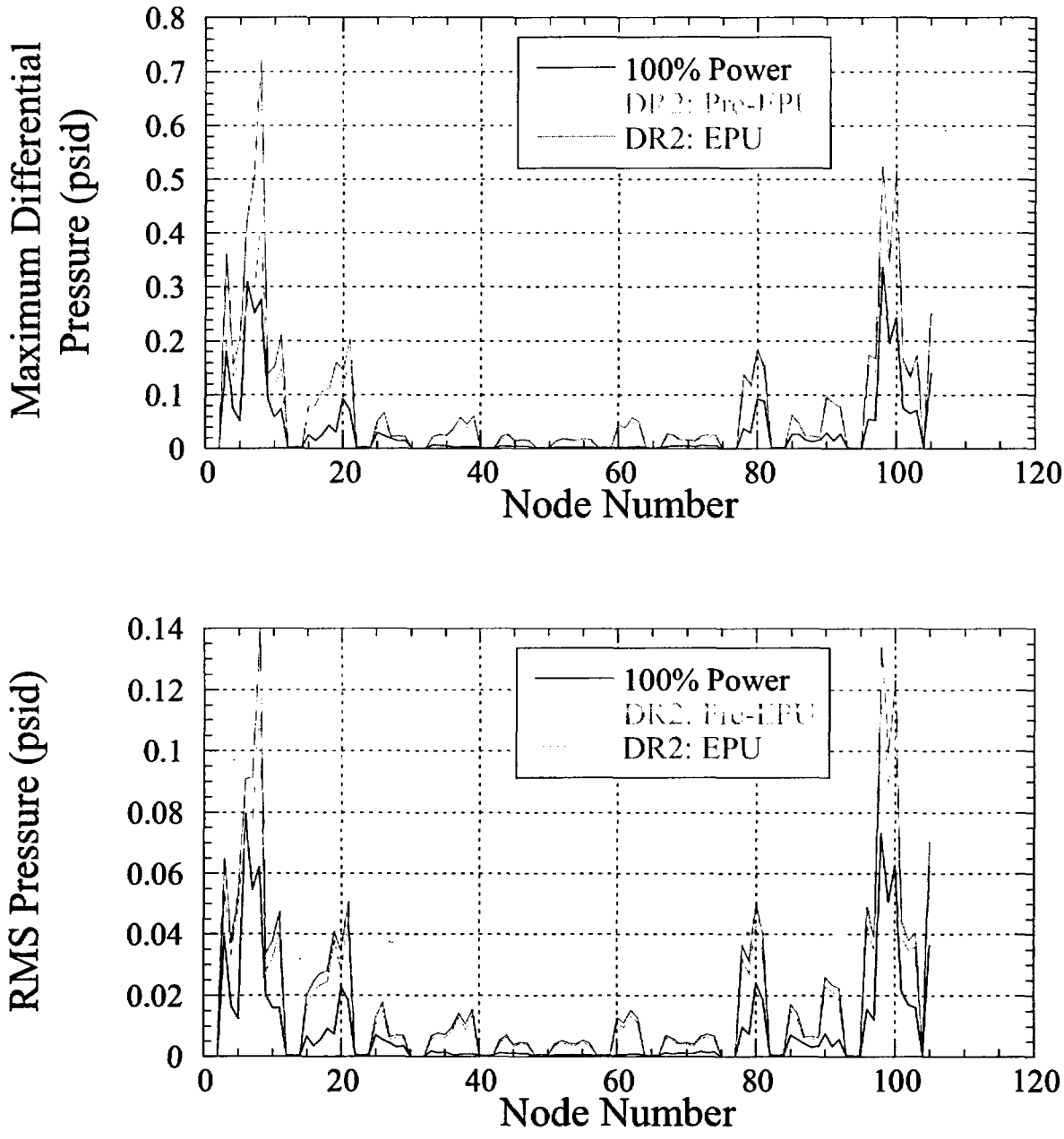

Figure 13. Low resolution grid mesh results for VY at 100% power (black curve), compared with DR2 at OLTP (red curve), and DR2 at EPU (blue curve), from [7].

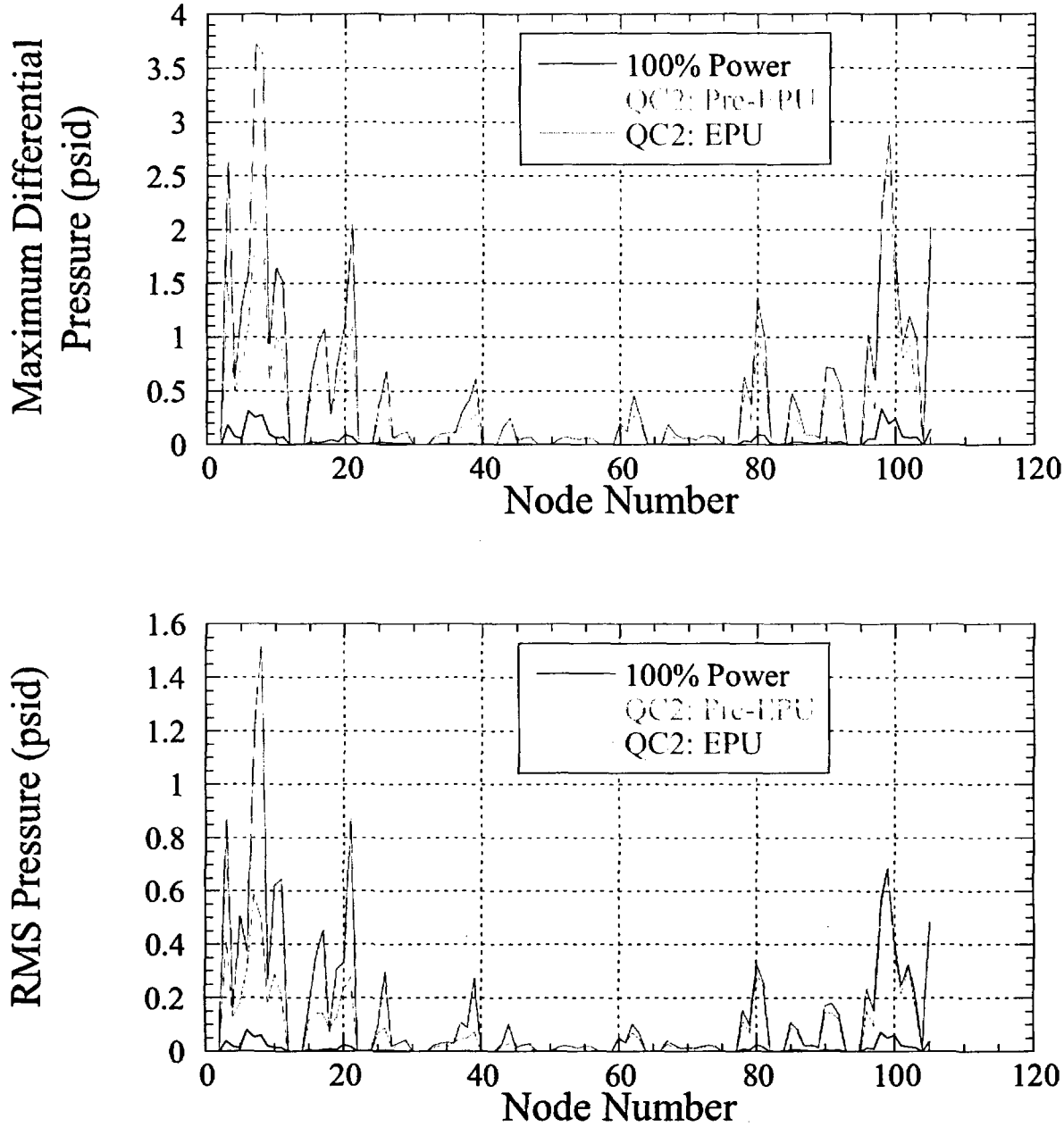

Figure 14. Low resolution grid mesh results for VY at 100% power (black curve), compared with QC2 at OLTP (red curve) and QC2 at EPU (blue curve), from [7].

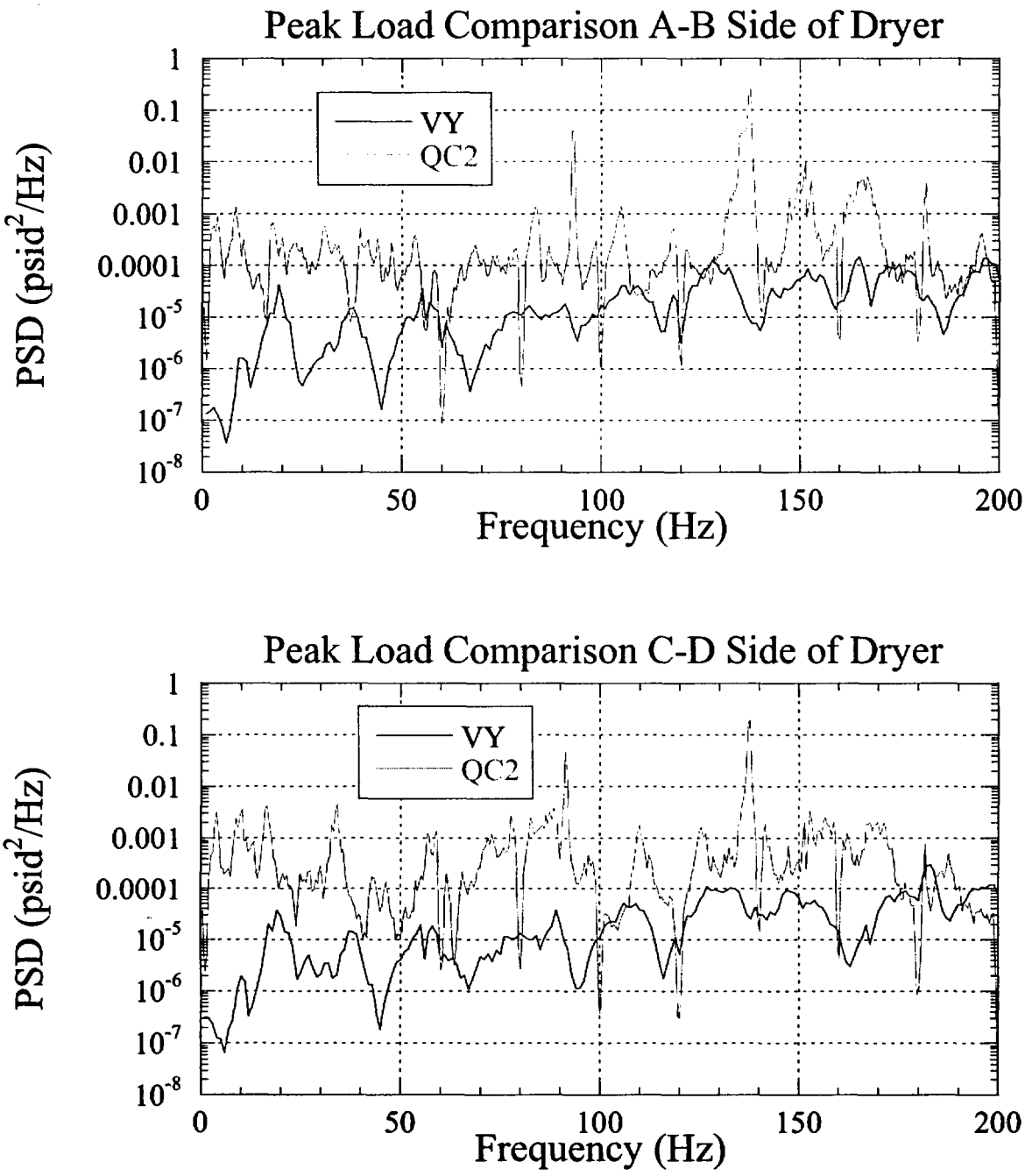

Figure 15. Comparison of peak loads for VY at 100% power (black curves) and peak loads for QC2 OLTP (blue curves): A-B side of dryer (top); C-D side of dryer (bottom).

SUMMARY BEHAVIOR WITH POWER SETTING

An indication of the effect of power level on the steam dryer may be seen in Figure 16, where the maximum differential pressure and RMS pressure are plotted as a function of power level. The effect of power level appears as an increase in pressure (although a small one), with 100% power giving the largest loads (these curves are consistent with Figure 9). Previously, in [4], it was thought that 90% power gave the highest steam dryer loads, but with the corrected venturi pressure time histories developed here, this result no longer holds. The reason for this may be traced to the conservatism built into the venturi instrument line analysis. The instrument line analysis is more accurate than what was developed previously [4] but includes conservatism that tends to increase dryer loads. This effect appears to be increasing as power level increases (Figure 16), although the actual increase in maximum differential pressure is small (0.075 psid on the A-B side of the dryer and 0.035 psid on the C-D side of the dryer from 90% to 100% power level).

Finally, VY results are compared against DR2 and QC2 results in Figure 17. The lower loads anticipated on VY are clearly seen (DR2 and VY analyses include strain gage data; QC2 results do not). This figure summarizes the behavior of the three steam dryers examined, and illustrates that there is little load difference expected for VY and DR2 as a function of feed flow rate (also percentage power in VY), but significant load difference expected for QC2.

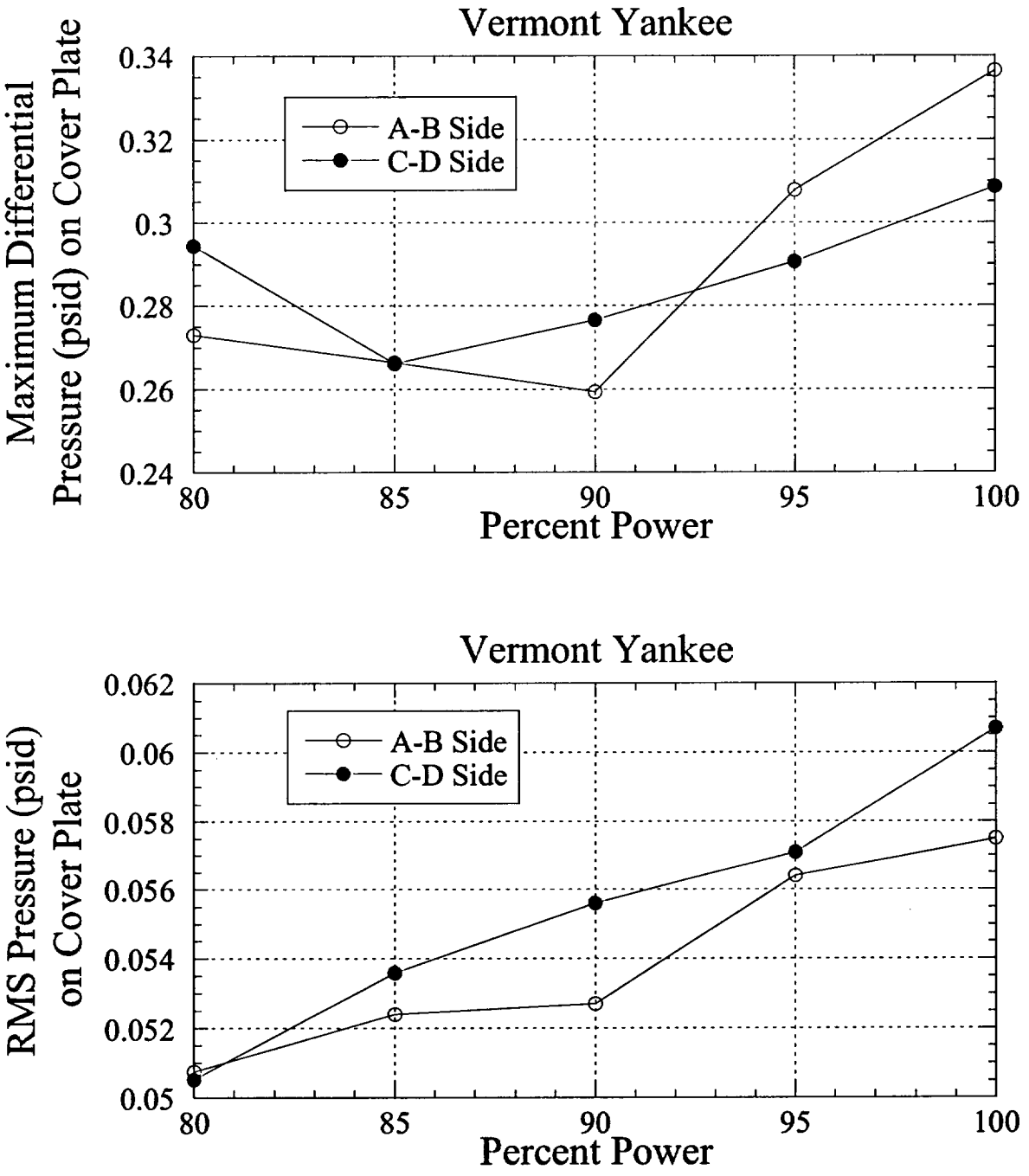

Figure 16. Summary comparison of maximum dryer pressure loads at VY as a function of power level.

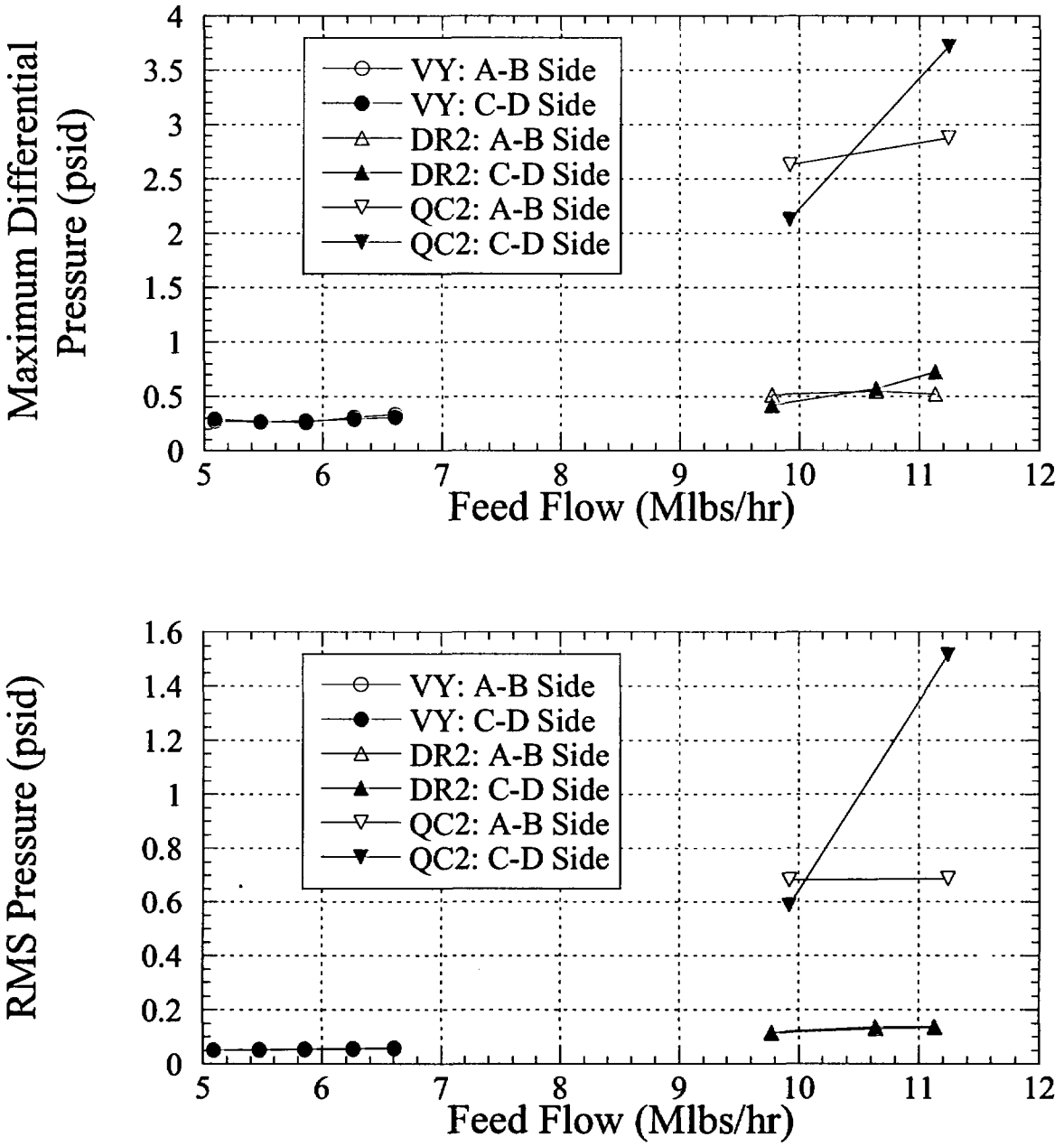

Figure 17. Comparison of maximum differential pressure loads and RMS for VY, DR2, and QC2 to 200 Hz.

QUALITY ASSURANCE

The work documented in this report meets requirements of Continuum Dynamics, Inc.'s Nuclear Quality Assurance Program.

REFERENCES

1. Continuum Dynamics, Inc. 2005. Acoustic Circuit Analysis of Vermont Yankee Instrument Lines (Rev. 0). C.D.I. Technical Memorandum No. 05-05.

2. Continuum Dynamics, Inc. 2004. Test Report for Validating an Instrument Line Acoustic Transmission Model (Rev. 0). C.D.I. Report No. 04-12.

3. Continuum Dynamics, Inc. 2005. Methodology to Determine Unsteady Pressure Loading on Components in Reactor Steam Domes (Rev. 6). C.D.I. Report No. 04-09 (Proprietary).

4. Continuum Dynamics, Inc. 2005. Hydrodynamic Loads on Vermont Yankee Steam Dryer (Rev. 0). C.D.I. Report No. 04-13.

5. Press, W. H., S. A. Teukolsky, W. T. Vettering, and B. P. Flannery. 1992. Numerical Recipes in FORTRAN: The Art of Scientific Computing. Second Edition. Cambridge University Press. 498-502, 542-551.

6. Schlichting, H. 1968. Boundary-Layer Theory. Sixth Edition. McGraw-Hill. 419-421.

7. Continuum Dynamics, Inc. 2005. Revised Hydrodynamic Loads on Quad Cities Unit 2 Steam Dryer to 200 Hz, with Comparison to Dresden Unit 2 and Dresden Unit 3 Loads (Rev. 0). C.D.I. Report No. 05-01.

8. Structural Integrity Associates, Inc. 2005. Report No. SIR-05-045 (Rev. A).

APPENDIX: VY HIGH RESOLUTION GRID MESH

Model predictions are collected into ASCII data files containing the time history data for the predictions of differential pressure (psid) across various locations on the plates in the dryer. A cross-sectional schematic of the dryer geometry is shown in Figure 7. Perspective views of the steam dryer panels are provided in Figure 8.

For horizontal plates, pressure differences are computed by subtracting the pressure below the plate from the pressure above the plate. For vertical plates, pressure differences are computed by subtracting the pressure to the right of the plate from the pressure to the left of the plate, for the vertical plates on the MSL C and D side, and in the opposite direction on the MSL A and B side (the direction designated "left" faces MSL C and D; "right" faces MSL A and B). For skirt plates, pressure differences are computed by subtracting the pressure inside the skirt from the pressure outside the skirt. Pressure differences are provided at all plate intersections, and along the steam dryer centerline (the 90° and 270° directions).

Each output file contains 2.5 seconds of data with a time difference of 0.0009765625 seconds to extract results to 200 Hz. There are 105 columns of data:

1. Time (seconds)
2. Pressure difference across the skirt at the steam dryer centerline below MSL C and D at the nominal water level (Figure 8d)
3. Pressure difference at the skirt and cover plate intersection at the steam dryer centerline below MSL C and D (Figures 8a and 8d)
4. Pressure difference across the skirt on the MSL B-C side below the E outer bank hood at the nominal water level (Figure 8d)
5. Pressure difference across the skirt on the MSL A-D side below the E outer bank hood at the nominal water level (Figure 8d)
6. Pressure difference across the skirt and the E outer bank hood on the MSL B-C side at the cover plate intersection (Figures 8a, 8c, and 8d)
7. Pressure difference across the E outer bank hood at the steam dryer centerline at the cover plate intersection (Figures 8a and 8c)
8. Pressure difference across the skirt and the E outer bank hood on the MSL A-D side at the cover plate intersection (Figures 8a, 8c, and 8d)
9. Pressure difference across the skirt and the E outer bank hood on the MSL B-C side at the top plate intersection (Figures 8b, 8c, and 8d)
10. Pressure difference across the E outer bank hood at the steam dryer centerline at the top plate intersection (Figures 8b and 8c)
11. Pressure difference across the skirt and the E outer bank hood on the MSL A-D side at the top plate intersection (Figures 8b, 8c, and 8d)
12. Pressure difference across the E bottom plate open edge at the skirt on the MSL B-C side (Figure 8a)
13. Pressure difference across the E bottom plate open edge at the steam dryer centerline (Figure 8a)
14. Pressure difference across the E bottom plate open edge at the skirt on the MSL A-D side (Figure 8a)

15. Pressure difference across the E top plate corner edge at the skirt on the MSL B-C side (Figure 8b)
16. Pressure difference across the E top plate corner edge at the steam dryer centerline (Figure 8b)
17. Pressure difference across the E top plate corner edge at the skirt on the MSL A-D side (Figure 8b)
18. Pressure difference across the skirt on the MSL B-C side below the D inner bank hood at the nominal water level (Figure 8d)
19. Pressure difference across the skirt on the MSL A-D side below the D inner bank hood at the nominal water level (Figure 8d)
20. Pressure difference across the skirt on the MSL B-C side at the D inner bank hood intersection with the E bottom plate (Figure 8d)
21. Pressure difference across the skirt on the MSL A-D side at the D inner bank hood intersection with the E bottom plate (Figure 8d)
22. Pressure difference across the D inner bank hood on the MSL B-C side at the E bottom plate intersection (Figures 8a and 8c)
23. Pressure difference across the D inner bank hood at the steam dryer centerline at the E bottom plate intersection (Figures 8a and 8c)
24. Pressure difference across the D inner bank hood on the MSL A-D side at the E bottom plate intersection (Figures 8a and 8c)
25. Pressure difference across the skirt on the MSL B-C side at the D inner bank hood intersection with the D top plate (Figure 8d)
26. Pressure difference across the skirt on the MSL A-D side at the D inner bank hood intersection with the D top plate (Figure 8d)
27. Pressure difference across the D inner bank hood on the MSL B-C side at the D top plate intersection (Figures 8b and 8c)
28. Pressure difference across the D inner bank hood at the steam dryer centerline at the D top plate intersection (Figures 8b and 8c)
29. Pressure difference across the D inner bank hood on the MSL A-D side at the D top plate intersection (Figures 8b and 8c)
30. Pressure difference across the D bottom plate open edge at the skirt on the MSL B-C side (Figure 8a)
31. Pressure difference across the D bottom plate open edge at the steam dryer centerline (Figure 8a)
32. Pressure difference across the D bottom plate open edge at the skirt on the MSL A-D side (Figure 8a)
33. Pressure difference across the D top plate open edge at the skirt on the MSL B-C side (Figure 8b)
34. Pressure difference across the D top plate open edge at the steam dryer centerline (Figure 8b)
35. Pressure difference across the D top plate open edge at the skirt on the MSL A-D side (Figure 8b)
36. Pressure difference across the skirt on the MSL B-C side below the C inner bank hood on the MSL C/D side at the nominal water level (Figure 8d)
37. Pressure difference across the skirt on the MSL A-D side below the C inner bank hood on the MSL C/D side at the nominal water level (Figure 8d)

38. Pressure difference across the skirt on the MSL B-C side at the C inner bank hood intersection with the D bottom plate (Figure 8d)
39. Pressure difference across the skirt on the MSL A-D side at the C inner bank hood intersection with the D bottom plate (Figure 8d)
40. Pressure difference across the C inner bank hood on the MSL B-C side at the D bottom plate intersection (Figures 8a and 8c)
41. Pressure difference across the C inner bank hood at the steam dryer centerline at the D bottom plate intersection (Figures 8a and 8c)
42. Pressure difference across the C inner bank hood on the MSL A-D side at the D bottom plate intersection (Figures 8a and 8c)
43. Pressure difference across the skirt on the MSL B-C side at the C inner bank hood intersection with the C top plate on the MSL C-D side (Figure 8d)
44. Pressure difference across the skirt on the MSL A-D side at the C inner bank hood intersection with the C top plate on the MSL C-D side (Figure 8d)
45. Pressure difference across the C inner bank hood on the MSL B-C side at the C top plate intersection on the MSL C-D side (Figures 8b and 8c)
46. Pressure difference across the C inner bank hood at the steam dryer centerline at the C top plate intersection on the MSL C-D side (Figures 8b and 8c)
47. Pressure difference across the C inner bank hood on the MSL A-D side at the C top plate intersection on the MSL C-D side (Figures 8b and 8c)
48. Pressure difference across the C bottom plate open edge at the skirt on the MSL B-C side on the MSL C-D side (Figure 8a)
49. Pressure difference across the C bottom plate open edge at the steam dryer centerline on the MSL C-D side (Figure 8a)
50. Pressure difference across the C bottom plate open edge at the skirt on the MSL A-D side on the MSL C-D side (Figure 8a)
51. Pressure difference across the C top plate open edge at the skirt on the MSL B-C side on the MSL C-D side (Figure 8b)
52. Pressure difference across the C top plate open edge at the steam dryer centerline on the MSL C-D side (Figure 8b)
53. Pressure difference across the C top plate open edge at the skirt on the MSL A-D side on the MSL C-D side (Figure 8b)
54. Pressure difference across the C top plate open edge at the skirt on the MSL B-C side on the MSL A-B side (Figure 8b)
55. Pressure difference across the C top plate open edge at the steam dryer centerline on the MSL A-B side (Figure 8b)
56. Pressure difference across the C top plate open edge at the skirt on the MSL A-D side on the MSL A-B side (Figure 8b)
57. Pressure difference across the C bottom plate open edge at the skirt on the MSL B-C side on the MSL A-B side (Figure 8a)
58. Pressure difference across the C bottom plate open edge at the steam dryer centerline on the MSL A-B side (Figure 8a)
59. Pressure difference across the C bottom plate open edge at the skirt on the MSL A-D side on the MSL A-B side (Figure 8a)
60. Pressure difference across the skirt on the MSL B-C side below the C inner bank hood on the MSL A-B side at the nominal water level (Figure 8d)

61. Pressure difference across the skirt on the MSL A-D side below the C inner bank hood on the MSL A-B side at the nominal water level (Figure 8d)
62. Pressure difference across the skirt on the MSL B-C side at the C inner bank hood intersection with the B bottom plate (Figure 8d)
63. Pressure difference across the skirt on the MSL A-D side at the C inner bank hood intersection with the B bottom plate (Figure 8d)
64. Pressure difference across the C inner bank hood on the MSL B-C side at the B bottom plate intersection (Figures 8a and 8c)
65. Pressure difference across the C inner bank hood at the steam dryer centerline at the B bottom plate intersection (Figures 8a and 8c)
66. Pressure difference across the C inner bank hood on the MSL A-D side at the B bottom plate intersection (Figures 8a and 8c)
67. Pressure difference across the skirt on the MSL B-C side at the C inner bank hood intersection with the C top plate on the MSL A-B side (Figure 8d)
68. Pressure difference across the skirt on the MSL A-D side at the C inner bank hood intersection with the C top plate on the MSL A-B side (Figure 8d)
69. Pressure difference across the C inner bank hood on the MSL B-C side at the C top plate intersection on the MSL A-B side (Figures 8b and 8c)
70. Pressure difference across the C inner bank hood at the steam dryer centerline at the C top plate intersection on the MSL A-B side (Figures 8b and 8c)
71. Pressure difference across the C inner bank hood on the MSL A-D side at the C top plate intersection on the MSL A-B side (Figures 8b and 8c)
72. Pressure difference across the B top plate open edge at the skirt on the MSL B-C side (Figure 8b)
73. Pressure difference across the B top plate open edge at the steam dryer centerline (Figure 8b)
74. Pressure difference across the B top plate open edge at the skirt on the MSL A-D side (Figure 8b)
75. Pressure difference across the B bottom plate open edge at the skirt on the MSL B-C side (Figure 8a)
76. Pressure difference across the B bottom plate open edge at the steam dryer centerline (Figure 8a)
77. Pressure difference across the B bottom plate open edge at the skirt on the MSL A-D side (Figure 8a)
78. Pressure difference across the skirt on the MSL B-C side below the B inner bank hood at the nominal water level (Figure 8d)
79. Pressure difference across the skirt on the MSL A-D side below the B inner bank hood at the nominal water level (Figure 8d)
80. Pressure difference across the skirt on the MSL B-C side at the B inner bank hood intersection with the A bottom plate (Figure 8d)
81. Pressure difference across the skirt on the MSL A-D side at the B inner bank hood intersection with the A bottom plate (Figure 8d)
82. Pressure difference across the B inner bank hood on the MSL B-C side at the A bottom plate intersection (Figures 8a and 8c)
83. Pressure difference across the B inner bank hood at the steam dryer centerline at the A bottom plate intersection (Figures 8a and 8c)

84. Pressure difference across the B inner bank hood on the MSL A-D side at the A bottom plate intersection (Figures 8a and 8c)
85. Pressure difference across the skirt on the MSL B-C side at the B inner bank hood intersection with the B top plate (Figure 8d)
86. Pressure difference across the skirt on the MSL A-D side at the B inner bank hood intersection with the B top plate (Figure 8d)
87. Pressure difference across the B inner bank hood on the MSL B-C side at the B top plate intersection (Figures 8b and 8c)
88. Pressure difference across the B inner bank hood at the steam dryer centerline at the B top plate intersection (Figures 8b and 8c)
89. Pressure difference across the B inner bank hood on the MSL A-D side at the B top plate intersection (Figures 8b and 8c)
90. Pressure difference across the A top plate corner edge at the skirt on the MSL B-C side (Figure 8b)
91. Pressure difference across the A top plate corner edge at the steam dryer centerline (Figure 8b)
92. Pressure difference across the A top plate corner edge at the skirt on the MSL A-D side (Figure 8b)
93. Pressure difference across the A bottom plate open edge at the skirt on the MSL B-C side (Figure 8a)
94. Pressure difference across the A bottom plate open edge at the steam dryer centerline (Figure 8a)
95. Pressure difference across the A bottom plate open edge at the skirt on the MSL A-D side (Figure 8a)
96. Pressure difference across the skirt on the MSL B-C side below the A outer bank hood at the nominal water level (Figure 8d)
97. Pressure difference across the skirt on the MSL A-D side below the A outer bank hood at the nominal water level (Figure 8d)
98. Pressure difference across the skirt and the A outer bank hood on the MSL B-C side at the cover plate intersection (Figures 8a, 8c, and 8d)
99. Pressure difference across the A outer bank hood at the steam dryer centerline at the cover plate intersection (Figures 8a and 8c)
100. Pressure difference across the skirt and the A outer bank hood on the MSL A-D side at the cover plate intersection (Figures 8a, 8c, and 8d)
101. Pressure difference across the skirt and the A outer bank hood on the MSL B-C side at the top plate intersection (Figures 8b, 8c, and 8d)
102. Pressure difference across the A outer bank hood at the steam dryer centerline at the top plate intersection (Figures 8b and 8c)
103. Pressure difference across the skirt and the A outer bank hood on the MSL A-D side at the top plate intersection (Figures 8b, 8c, and 8d)
104. Pressure difference across the skirt at the steam dryer centerline below MSL A and B at the nominal water level (Figure 8d)
105. Pressure difference at the skirt and cover plate intersection at the steam dryer centerline below MSL A and B (Figures 8a and 8d)

The grid used for the Helmholtz solver for pressure is a rectangular grid with spacing of 3 inches in all three directions. The grid coordinate system is x and y horizontal (x points toward 90° and y points toward 0°) and zero at the center of the dryer, with z out of the paper in Figure 7 and zero at the steam-water interface. The 104 low-resolution nodes are shown on these figures for reference. The bottom center of the steam dome (at the steam-water interface) has a coordinate of $n_x = 37$, $n_y = 37$, and $n_z = 1$. The cover plate is at the level height of $n_z = 26$, while the outer hood top plate is at the level height of $n_z = 47$.

The transmitted data files contain a title to each column of data. The first column in each file is time (in seconds), designated by the title "0", and numerous additional columns titled with a number. For every pressure difference provided, its location is designated by multiplying its x grid location (n_x) by 10000, adding its y grid location (n_y) multiplied by 100, and adding its z grid location (n_z). Thus, for example, the heading 713726 corresponds to $n_x = 71$, $n_y = 37$, and $n_z = 26$, and is the position of node 105 in the low-resolution grid. Node 2 is 33702.

The transmitted data files consist of four sets: AB (for the A-B main steam line side of the steam dome), CD (for the C-D main steam line side of the steam dome), and ML and EX (for the middle of the dryer).